Trapped Disturbances and Effects of Tropopause Height in Stratified Flow over Topography

by

Kahn Yung Lim

B.S. University of California, Los Angeles, 1999

Submitted to the Department of Mechanical Engineering in partial fulfillment of the requirements for the degree of

Master of Science in Mechanical Engineering

at the
Massachusetts Institute of Technology

February 2001

Signature of Author _____
Department of Mechanical Engineering
January 15, 2001

Certified by _____
Triantaphyllos R. Akylas
Thesis Supervisor

Accepted by _____
Ain A. Sonin
Chairman, Departmental Committee for Graduate Studies

Trapped Disturbances and Effects of Tropopause Height in Stratified Flow over Topography

by

Kahn Yung Lim

Suubmitted to the Department of Mechanical Engineering
On January 15, 2001 in Partial Fulfillment of the
Requirement for the Degree of Master of Science in
Mechanical Engineering

ABSTRACT

Periodic disturbance in Brunt-Väisälä frequency (BVF) can have significant influence on stratified flow over topography. Its influences include wave trapping and wave instability, depending on its wavelength, its phase, and its amplitude. This thesis shows the existence of a critical phase for some stratified flows. At critical phase or phase close to it, flow instability occurs. In addition, this thesis shows the periodic disturbance has larger influence in the two-dimensional flow, very little influence on three-dimensional flow with round topography, and some influence on three-dimensional flow with large spanwise topography.

Tropopause height also affects stratified flow. A set of atmospheric data was examined closely for the wave perturbation caused by the tropopause height. Numerical simulations indicate that under the conditions given by the data, the generated mountain-wave disturbance is most active when the tropopause height is in the range of 10.5-14km. The actual flow data reveals that regions, where the tropopause height is around 10-11km, experience high wave activity.

Thesis Supervisor: Triantaphyllos R. Akylas
Title: Professor of Mechanical Engineering

ACKNOWLEDGEMENTS

The author would like to thank his advisor, Professor Akylas, for providing the theory of the two- and three-dimensional stratified fluid flow. In addition, he has provided timely guidance and useful comments to the work presented in this thesis.

David Calvo has also been a great help in assisting the author with the numerical simulation. With his help, the author was able to use unequal spacing to speed up the two-dimensional numerical computation.

Also a special thank is due to Professor Smith in assisting the author with the numerical simulation of the linear three-dimensional flow.

The author would finally like to thank his family and Phung Tran for being very supportive in all his endeavors.

Effort supported by the Air Force Office of Scientific Research, Air Force Materials Command, USAF, under Grant Number FA9620-98-1-0388.

TABLE OF CONTENTS

LIST OF FIGURES

Chapter One

Introduction

The motion of stratified fluid such as airflow makes big and small impacts in our daily life. People living in the upper eastern United States know that a beautiful morning can quickly become a dark gloomy afternoon with snow blanketing everything in sight. A sudden shift of weather catches people off guard, creates havoc for farmers, and on a few occasions causes mass destruction of properties and death. Such unpredictability leaves us asking the question, is weather forecasting a science or an art? Predicting weather is a behemoth task that includes the knowledge of many fields of studies. Understanding stratified fluid flow is an integral part of it.

Stratified fluid is a fluid that has a density gradient. Earth's atmosphere and ocean are the two notable examples of the stratified fluid. Their density gradient is a result of the effect of gravity. In this thesis, the density gradient is introduced through the quantity called the Brunt-Väisälä frequency (BVF). This quantity is the frequency at which a small fluid element oscillates vertically about its equilibrium position and it is defined as

$$N(z) = \sqrt{-g\frac{\rho_z}{\rho}}$$

The density gradient appears in the numerator and the density itself appears in the denominator, g being the gravitational acceleration. The case where BVF is constant has practical importance due to the fact that a typical atmospheric BVF profile approximately consists of layers of constant BVF. For BVF to be constant, the fluid density must vary exponentially with height. Its effects on the stratified fluid are the basis for this thesis.

Yet we know only so much about this opaque but ubiquitous medium. There is a good reason. The set of equations that describes the stratified fluid is called the Navier Stokes equation and the first and second law of thermodynamics. This set of governing equations is so complex that even with the current ultra-fast supercomputer, no one has been able to deduce its solution in its entirety. This thesis will examine the stratified flow based on a much simplified but practical set of governing equations.

The simplified governing equations describe the stratified fluid at the scale of the atmospheric level with the internal gravity-waves generated by flowing over a topography. This flow can be considered inviscid, incompressible and steady. Large-scale flow is inviscid as long as the boundary layer does not separate. Moreover, the internal gravity wave does not reach anywhere close to the speed of sound. So, the flow is further simplified by making it incompressible. Moreover, the incoming flow is assumed to have a uniformed profile.

Long (1953) made a systematic study of stratified flow with constant BVF. The model he used for his research has been the foundation for stratified flow since. In Long's model, the governing equations for both the small and finite-amplitude flows are linear as a result of BVF being constant and independent of height. Furthermore, the model applies in regions where wave breaking does not occur.

Since then, researchers have built on Long's model by using various BVF profiles to make the model an even more realistic one. Atmospheric BVF profile usually has two or three layers of constant BVF. Section 4 of the appendix shows several examples of the atmospheric BVF profile. Durran (1992) developed a simple two-layer model. Davis (1999) extends the two-layer model to a model with variable BVF profile. By further

modifying the BVF profile with a periodic disturbance, a fascinating phenomenon of wave getting trapped closed to the topography occurs. In the atmosphere, BVF is only approximately constant in each layer. It has a great amount of small-amplitude disturbances. When that disturbance is periodic with a certain wavelength, numerical simulations suggest wave trapping to occur.

Two notable papers have been published on stratified flow with periodic disturbance in the BVF profile. Phillips (1968) pointed out that when the vertical wave number of the periodic disturbance is twice the ratio of the incoming flow velocity to the BVF, waves in stratified fluid get trapped near its source. Kantzios and Akylas (1993) also pointed out that when there is a periodic disturbance in the fluid stratification, the wave decreases as it moves farther away from the source.

This thesis continues the investigation on the effect of the periodic disturbance on the stratified fluid. The investigation will use nonlinear two-dimensional and linear three-dimensional models to represent the stratified flow. In the conclusion of the study, the results will show that the periodic perturbation, defined by its amplitude, phase, and wavelength, has important and unique influences on the stratified flow.

Another part of this thesis is to analyze the atmospheric data provided by the Air Force. Durran (1992) and Klemp and Lilly (1975) pointed out that the tropopause height can have a significant influence on flow over topography. Klemp and Lilly (1975) also made field observations in the region around Boulder, Colorado. In that region, the wind blowing over the mountain toward the city has caused structural damage to a large number of buildings. They observed that given certain atmospheric conditions like the location of the tropopause and the BVF, the wind speed close to the ground increases.

Durran (1992) developed a simple two-layer model to explore the effects that the tropopause can have on stratified flow over topography. He compared the differences between the linear and non-linear equations of motion in the vicinity of the tuned tropopause. The linear governing equations show that the tropopause becomes tuned at regular intervals in the vertical direction. Unlike the linear case, the non-linear governing equation places the tuned tropopause at irregular intervals in the vertical direction. Davis (1999) extends the simple two-layer model of constant BVF to a model with variable BVF. He also found that tuning of the tropopause is possible.

Since then, additional atmospheric data have become available. Based on these data, the present work explores the effects of the tropopause on the induced gravity-wave disturbances.

Chapter two gives the two-dimensional stratified flow theory and discusses the numerical results in regards to the effects of the periodic disturbance. Chapter three discusses the three dimensional flow. Chapter four examines the atmospheric data for the effects of the tropopause height and presents its conclusion.

Chapter Two

Two dimensional stratified flow

Section 2.1 provides the theory and the foundation of two-dimensional stratified fluid flow in large depth over topography. The general theory is presented first and the discussion of small-amplitude and finite-amplitude flows follows. Section 2.2 gives numerical results related to the investigation of the periodic disturbance in BVF on stratified flow.

2.1 Theory

Using conservation of mass and momentum with the assumptions mentioned in the introduction, the governing equations for the stratified fluid flow in large depth are,

$$\nabla \cdot \vec{u} = 0 \tag{2.1}$$

$$\vec{u} \cdot \nabla \rho = 0 \tag{2.2}$$

$$\rho \vec{u} \cdot \nabla \vec{u} = -\nabla p + \rho \vec{g} \tag{2.3}$$

It is convenient to introduce dimensionless variables, eliminate pressure and combine the resulting quantities to form a single governing equation. The dimensionless variables used are

$$x = L\tilde{x},\ z = \frac{U_o}{N_o}\tilde{z},\ u = U_o\tilde{u},\ w = \frac{U_o^2}{LN_o}\tilde{w},\ \rho = \rho_o\tilde{\rho},\ p = \frac{gU_o\rho_o}{N_o}\tilde{p} \tag{2.4}$$

L represents the characteristic length of the topography width. U_o represents the nominal horizontal incoming velocity. N_o represents the nominal BVF. The resulting equation is,

$$\Psi_{zz} + N^2(\Psi)(z - \Psi) + \mu^2\Psi_{xx} + \frac{\beta}{2}N^2(\Psi)\left(\Psi_z^2 + \mu^2\Psi_x^2 - 1\right) = 0. \tag{2.5}$$

The detail is worked out in the section 1 of the appendix. Ψ is the streamfunction and it is related to the velocity vector. The relationship is

$$u = \Psi_z,\ w = -\Psi_x$$

β, is called the Boussinesq parameter and it is related to the stratification of the fluid, μ is called the longwave number and it is related to the wave dispersion. These two quantities are defined below.

$$\beta = \frac{N_o U_o}{g},\ \mu = \frac{U_o}{N_o L} \tag{2.6}$$

Using Bossinessq approximation, which implies that $\beta \to 0$, and hydrostatic approximation, which implies that $\mu \to 0$, the governing equation, equation 2.5, simplifies to

$$\psi_{zz} + N^2(\psi + z)\psi = 0, \tag{2.7}$$

where $\psi = \Psi - z$ is the perturbation streamfunction. N is the dimensionless BVF and it is given in the appendix, section 1, equation A.1.17. For the stratified flow with two layers of constant BVF, N can be described by the following equation.

$$N = a + b\tanh(c(z-d)) \tag{2.8}$$

The constants a and b together define the value of BVF in the lower and upper layer. The constant, c, determines the size of the tropopause. The constant d is the tropopause height. Additional terms will be added to equation 2.8 to include the periodic background dsiturbance.

2.1.1 Small-amplitude stratified flow

In the small-amplitude stratified flow, equation 2.7 simplifies to

$$\psi_{zz} + N^2(z)\psi = 0 \tag{2.9}$$

The solution to equation 2.9 is,

$$\psi_1(x,z) = A(x)\eta_1(z) + B(x)\eta_2(z) \tag{2.10}$$

η_1 and η_2 are obtained by solving the following linear differential equation with its boundary conditions.

$$\frac{d^2\eta}{dz^2} + N^2(z)\eta(z) = 0 \tag{2.11}$$

$$\eta_1(0) = 1,\ \frac{d\eta_1}{dz}(0) = 0\ \eta_2(0) = 0\ \frac{d\eta_2}{dz}(0) = 1 \tag{2.12}$$

The subscript on ψ_1 in equation 2.10 emphasizes that it applies to the regions where N is a function of the height as well as when N is constant. In contrast, ψ_2, defined below, applies to the region where the stratified fluid must have constant BVF.

$$\psi_2(x,z) = C(x)\sin(N_\infty z_\infty) + D(x)\cos(N_\infty z_\infty) \tag{2.13}$$

So, ψ_1 is a more general solution than ψ_2 and when its coefficients are determined, ψ_1 will be the solution to the governing equation, equation 2.9.

The lower and upper boundary conditions are used to solve for the coefficients of ψ_1. The procedure is explained below.

The lower and upper boundary conditions are applied first. The upper boundary condition, also called the radiation condition, states that energy must propagate away from the source. In wave propagation, energy travels at group velocity. Thus group

velocity must be positive for the wave energy to move away from the topography. Group velocity for the stratified flow in large depth is,

$$c_{g,z} = \frac{\mathrm{sgn}(m)Nk}{m^2} \tag{2.14}$$

For equation 2.14 to be positive, wave numbers k and m must have the same sign. This can be expressed in the following way,

$$km > 0 \tag{2.15}$$

To use boundary condition in equation 2.15, the sine and cosine terms in equation 2.13 are first expressed in their exponential form and then they are transformed into the frequency domain using the Fourier transform. The resulting equation is,

$$\psi_2(x,z) = \frac{1}{2}\int_{-\infty}^{\infty}\left[\hat{D}(k) - i\hat{C}(k)\right]e^{i(kx+mz)} + \frac{1}{2}\int_{-\infty}^{\infty}\left[\hat{D}(k) + i\hat{C}(k)\right]e^{i(kx-mz)} \tag{2.16}$$

m is the vertical wave number which is

$$m = \frac{N}{U} \tag{2.17}$$

Equation 2.15 states that k and m must have the same sign and to satisfy this criteria, the following conditions must be true.

$$\hat{D}(k) = i\hat{C}(k) \qquad \text{for} \qquad k < 0, \tag{2.18}$$

$$\hat{D}(k) = -i\hat{C}(k) \qquad \text{for} \qquad k > 0. \tag{2.19}$$

This is equivalent to

$$\hat{D}(k) = -i\,\mathrm{sgn}(k)\hat{C}(k) \tag{2.20}$$

In real domain, this condition is,

$$C(x) = H[D(x)] \tag{2.21}$$

Equation 2.21 eliminates one variable by relating C and D. 'H' is the symbol for the Hilbert transform. It is defined as

$$\mathrm{H}[f(x)] = \frac{1}{\pi} \int_{-\infty}^{\infty} \frac{f(x')}{x'-x} dx' \tag{2.22}$$

The second of the two boundary conditions is the lower boundary condition. This condition states that fluid flowing adjacent to the topography cannot have normal velocity component. This is expressed in the following three equations.

$$\vec{u} \cdot \vec{n} = 0 \tag{2.23}$$

$$\vec{n} = \nabla F \tag{2.24}$$

$$F = z - f \tag{2.25}.$$

The two-dimensional topography is described by the following function.

$$f = \frac{h}{\left(1 + x^2\right)^{3/2}} \tag{2.26}$$

Combining equation 2.23, 2.24, 2.25, and 2.26 and expressing the result in streamline perturbation give equation 2.27, the working form of the lower boundary condition.

$$\psi_1(x,z)_{z=f} + z\big|_f = 0 \tag{2.27}.$$

To obtain the solution to the governing equation, ψ_1 and ψ_2 are combined using the following two conditions.

$$\psi_1(x,H) = \psi_2(x,H) \tag{2.28}$$

$$\psi_{1,z}(x,H) = \psi_{2,z}(x,H) \tag{2.29}$$

They state that the wave velocity and wave displacement for ψ_1 and ψ_2 must be matched in the height where the BVF is constant or does not change with height. The resulting

quantity is combined further by the lower and upper boundary conditions stated above. The following is the set of simultaneous equations.

$$-f\eta_1(H)+B\eta_2(H)=C\sin(N_\infty H)+D\cos(N_\infty H) \tag{2.30}$$

$$-f\eta_{1z}(H)+B\eta_{2z}(H)=CN_\infty\cos(N_\infty H)-DN_\infty\sin(N_\infty H) \tag{2.31}$$

$$C=H[D] \tag{2.32}$$

Once the coefficient B is found, ψ_1 is also found since A was found by applying the lower boundary condition.

2.1.2 Finite-amplitude stratified flow

For the finite-amplitude case, the solution cannot be obtained as easily. As stated previously, the governing equation is

$$\psi_{zz} + N^2(\psi + z)\psi = 0\,. \tag{2.33}$$

Iteration is required to obtain the solution. Unlike the small-amplitude case, the BVF (N) in this case depends on the perturbation ψ also. The first guess of ψ to start the iteration is the solution from the small-amplitude analysis. The upper boundary condition is applied next. Then, equation 2.7 is integrated down to the topography where the lower boundary condition is applied. A new guess of ψ is made using the Newton-Raphson iteration method. This process is continued until ψ satisfied the lower and upper boundary conditions.

All the numerical simulations on the two-dimensional stratified flow presented in this thesis are based on the solution to equation 2.33.

2.1.3 Addition of periodic disturbance to BVF profile

Flows with a periodic disturbance on its BVF profiles are a significant part of this thesis. This section explains the motivation behind adding a periodic disturbance to the BVF profile. Also a multiple scale analysis on the linear governing equation is done to show the existence of a resonance when the wavelength of the periodic disturbance is twice the ratio of the incoming wind velocity to the BVF.

In the actual atmospheric BVF, there exist substantial background disturbances. In the case when the disturbance is periodic and its wavelength is twice the ratio of the wind velocity to the BVF, Phillip (1968) and Kantzios and Akylas (1993) pointed out that the wave trapping occurs. To study this kind of flow, a sine function is added to the BVF profile. The resulting modified function describing this BVF is

$$N = [a + b\tanh(c(z-d))] + \left[\frac{A_p}{2}(1-\tanh(3(z-BH)))(\sin(Tz+\phi))\right] \tag{2.34}$$

The second bracket in equation 2.34 represents the newly added disturbance. T is the wavelength of the perturbation. ϕ is the phase of the perturbation. A is the amplitude of the perturbation. BH is the height when the perturbation stops with the BVF returning back to its undisturbed level.

A multiple scale analysis will be carried out on the following equation to demonstrate that resonance occurs when T is twice the ratio of the BVF to the incoming velocity.

$$\frac{d^2\eta}{dz^2} + \left(N_o + A_p \sin(Tz+\phi)\right)^2 \eta(z) = 0 \tag{2.35}$$

The magnitude of A_p is of the order of ε. The solution to equation 2.35 is

$$\psi = A(x)\eta_1 + B(x)\eta_2 \tag{2.36}$$

η_1 and η_2 are obtained by integrating equation 2.37 with its boundary conditions

$$\eta_{zz} + N^2(z)\eta = 0 \tag{2.37}$$

$$\begin{aligned} \eta_1(0) &= 0 \qquad \eta_2(0) = 1 \\ \eta_{1z}(0) &= 1 \qquad \eta_{2z}(0) = 0 \end{aligned} \tag{2.38}$$

The solution to the η_1 case is broken down using the multiple scale analysis and the first two orders solutions are

O(1): $$\eta_o = \frac{e^{iN_o z} + e^{-iN_o z}}{2} = \cos N_o z \tag{2.39}$$

O(ε^1): $$\eta_1 = -\frac{iE+F}{2i}e^{iN_o z} + \frac{F-iE}{2i}e^{-iN_o z} + \frac{2N_o A_p}{(T+N_o)^2 - N_o^2}\sin(Tz + \phi + N_o z)$$

$$+ \frac{2N_o A_p}{(T-N_o)^2 - N_o^2}\sin(Tz + \phi - N_o z) \tag{2.40}$$

The detail is given in section 2 of the appendix. E and F can also be found there. Equations 2.39 and 2.40 represent the solution of equation 2.34, with the accuracy at order one. The important result to note from the multiple scale analysis is that the last term in equation 2.40 shows that when T the wavelength of the sinusoid is twice the value of the dimensionless BVF, N_o, the linear solution does not exist. This signifies resonance condition in stratified fluid. The result agrees with Phillips (1968) and Kantzios and Akylas (1992).

2.2 Discussion

Previous section shows that the periodic disturbance on the BVF causes some sort of resonance in the stratified flow. But its actual effects are not clear. The task of the following three sections is to clarify the role of this periodic disturbance through the use of nonlinear numerical simulation.

2.2.1 Effects of the perturbation amplitude

In this section, a series of numerical simulations is performed to show the effects of the disturbance amplitude on the stratified flow. The simulation uses a BVF profile described by $a = 1.6$; $b = 0.6$; $c = 20$; $d = 3$ with the disturbance phase equal to $\pi/2$ and varies its amplitude from 0 to 0.4. This method of carrying out the numerical simulation will isolate the effects of the disturbance amplitude. The topography is set to 0.5.

Figure 2.1 shows two sets of streamlines, one with the disturbance and one without the disturbance. The solid streamlines, representing the flow without the disturbance, have larger wave activity than the dotted streamlines, which represent the flow with the disturbance amplitude at 0.4.

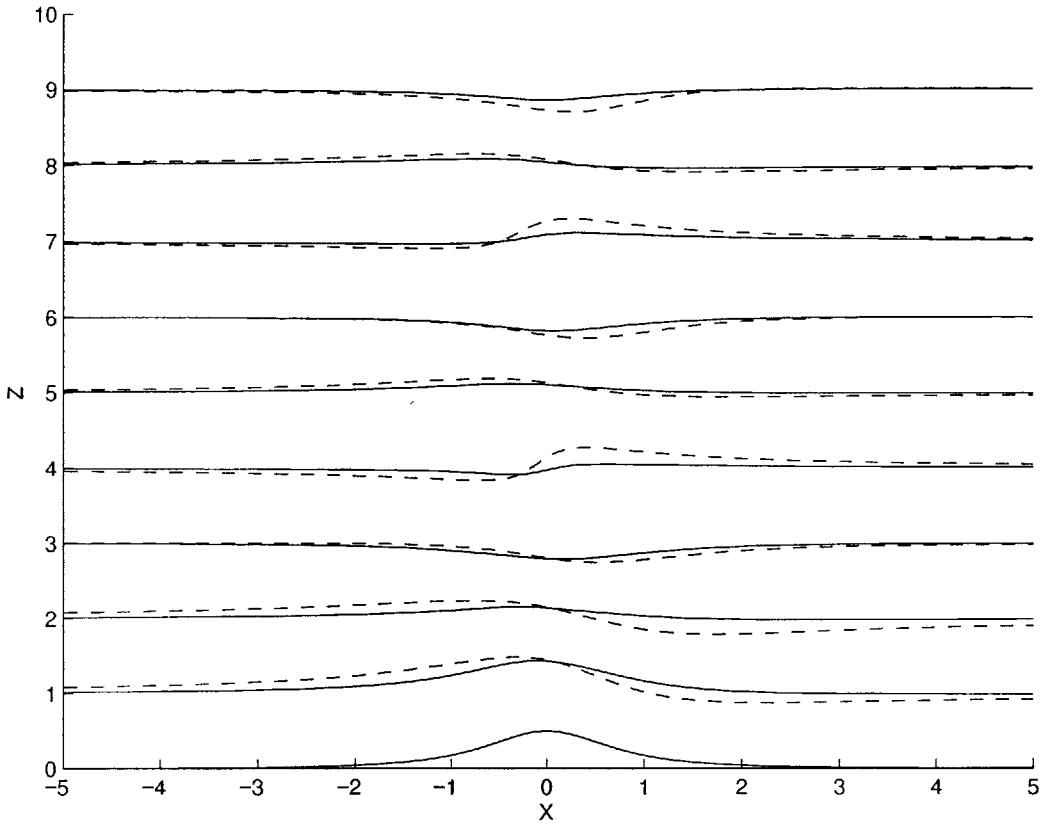

Figure 2.1: Flow with no background perturbation and flow with background perturbation.

The reduction of wave amplitude in the presence of disturbance is referred to as wave trapping. To further emphasize the wave trapping as a result of the disturbance, Figure 2.2 shows the wave activity as a function of the disturbance amplitude. The plot unequivocally shows that as the disturbance amplitude increases, the wave amplitude decreases.

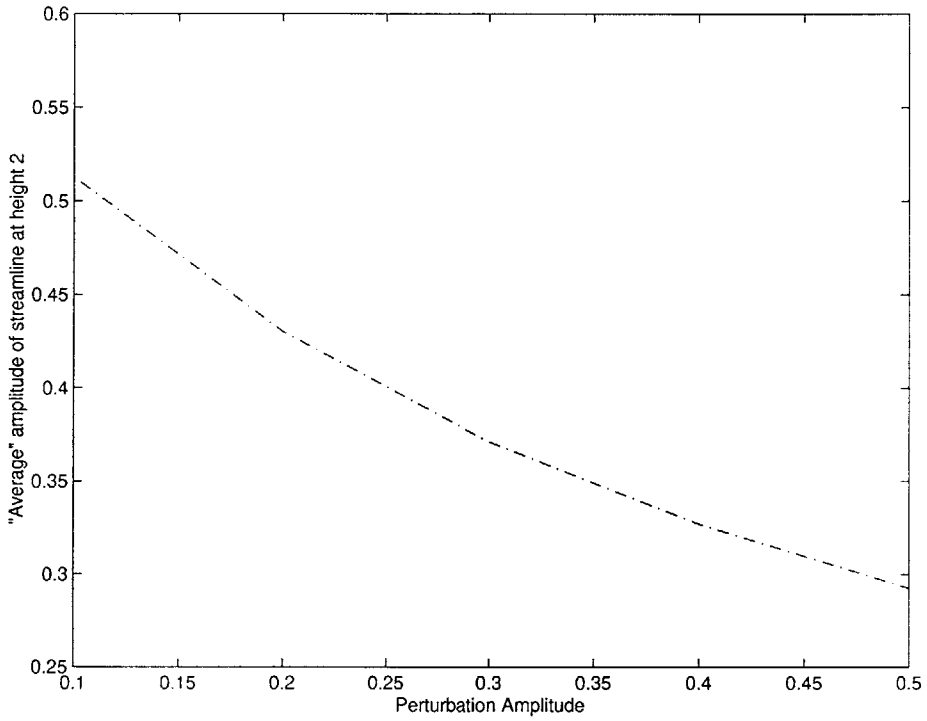

Figure 2.2: Effects of perturbation amplitude on generated waves.

To make Figure 2.2, the wave amplitudes from the second streamline are subtracted when the flow is undisturbed. The squared of the resulting quantities are summed and then the square root is taken. This method takes into account the negative as well as the positive wave amplitude with respect to the undisturbed level. If there were no disturbance, the normalized wave amplitude would be zero. This presentation allows an effective illustration of the wave activity as a function of the perturbation amplitude

2.2.2 Effects of the perturbation phase on waves in stratified flow

Previous section shows that the presence of the periodic disturbance in stratified fluid causes wave trapping. In this section, the other component of the periodic disturbance, the phase ϕ in equation 2.34, is investigated. Numerical simulations will

show that the phase can cause significant changes in the flows. In carrying out the following numerical simulation, the disturbance phase is varied from 0 to $\pi/2$ and its amplitude is kept constant at 0.1. This method isolates the influence of the disturbance phase on the stratified flow. In addition, the BVF profile for the simulation is described by $a = 1$; $b = 1/3$; $c = 20$; $d = 5$ and the topography height is set to 0.01. This topography is indeed very small but its resulting simulated flows will demonstrate that the disturbance phase does have a dramatic impact on the flow.

Numerical simulation shows that the flow with the BVF described above becomes unstable when its phase is near 0.13255 radian. 0.13255 is referred to as the critical disturbance phase. Figure 2.2 superposes two sets of flows, one with the disturbance phase at 0 radian and one with the phase at 0.1081 radian. The comparison brings out the dramatic effects of the phase when it is close to the critical value. The solid streamline, representing the flow with the phase at 0.1081 radian, shows large steepness in its waves. In contrast, the dotted streamline, representing the flow with the phase at zero, shows little steepness in its wave. Large steepness in the streamlines suggests that wave breaking is about to occur. For an even more dramatic comparison, stratified flow without the periodic disturbance to its BVF does not break until the topography height is beyond 0.85. This is eighty-five times larger than the topography that causes wave breaking in the flow with the disturbance phase near the critical value. This shows the tremendous impact the perturbation phase has on the stratified fluid.

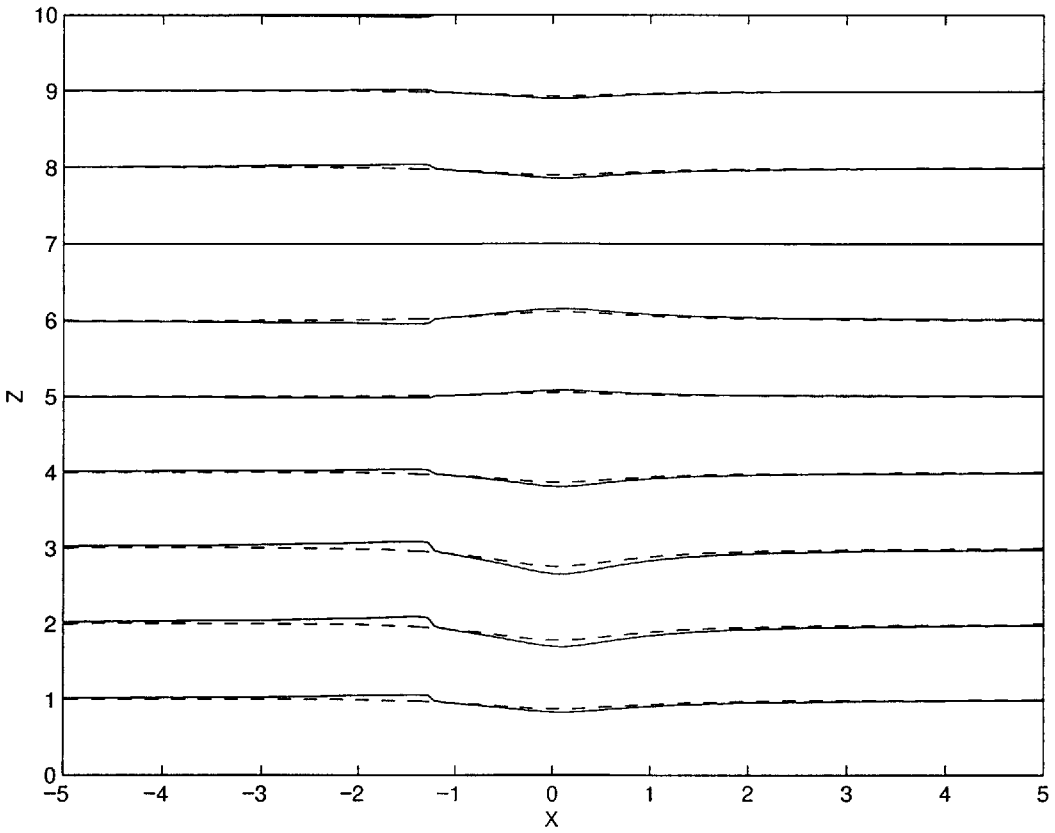

Figure 2.3: Streamlines with perturbation phase at 0.1081radian (solid) and 0 radian (dotted).

Figure 2.4 and 2.5 are made to summarize the relationship between the generated wave and the disturbance phase. They show clearly that as the disturbance phase moves closer to 0.13255 radian, wave activity increases. Looking at both figures together also shows that the generated wave is large or unstable when the phase is between 0.1081 radian and 0.1625radian. The author averages these two phases to obtain the critical value of 0.13255 radian. Therefore, this value is really an approximation.

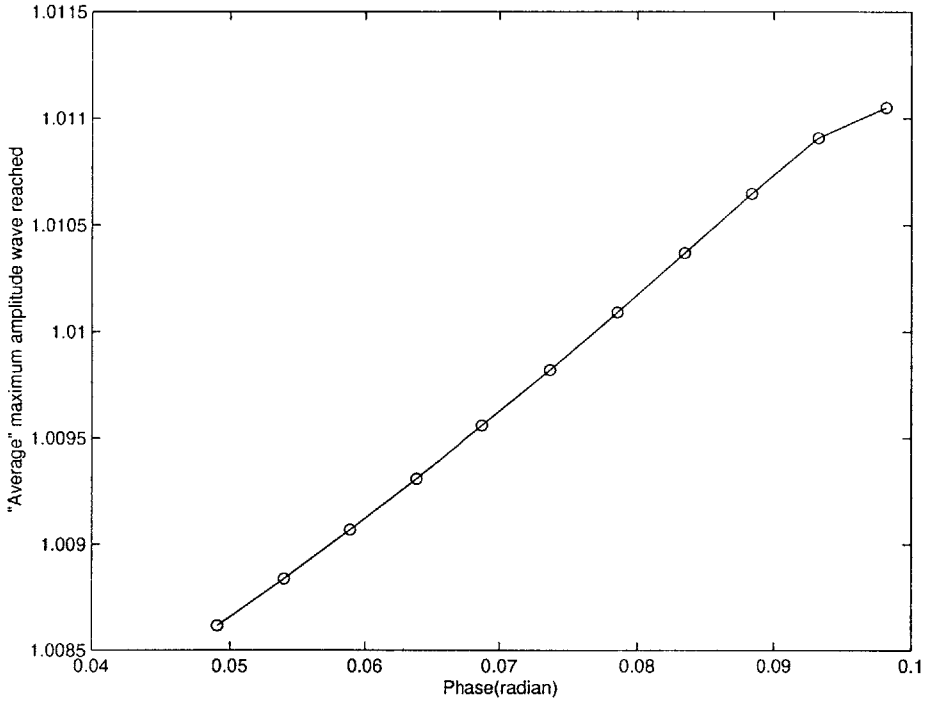

Figure 2.4: Wave amplitude versus disturbance phase: 0 → 0.13255 radian.

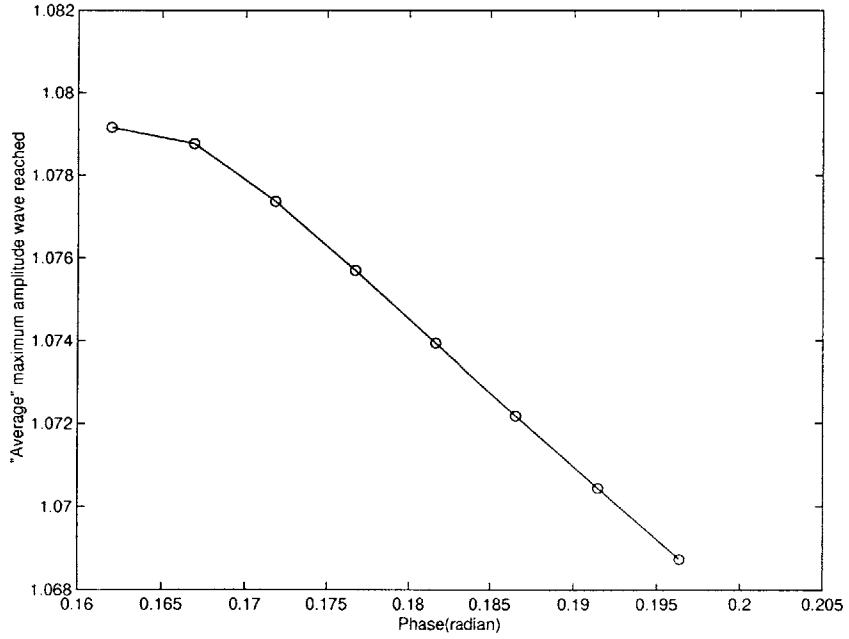

Figure 2.5: Wave amplitude versus disturbance phase: $\pi/2 \rightarrow 13255$ radian.

Figure 2.6 and Figure 2.7 are made by taking the maximum wave amplitude reached by the flow for each phase and plot it as a function of the phase (in an undisturbed flow, the maximum wave amplitude reached relative to the undisturbed level would be zero).

The existence of wave instability or resonance can also be further validated by closely examining the flow pattern when the perturbation phase is above the critical value and when it is below the critical value. Figure 2.5 shows the flow when the disturbance phase is at 0.1081 radian, which is below the critical value. For this flow, the large steepness in the wave occurs before the topography. In contrast, Figure 2.6 shows that when the phase is larger than 0.13255 radian, large steepness in the streamline occurs after the topography. The conclusion draws from the comparison of these two cases suggests a resonance occurring when the disturbance phase is around 0.13255 radian.

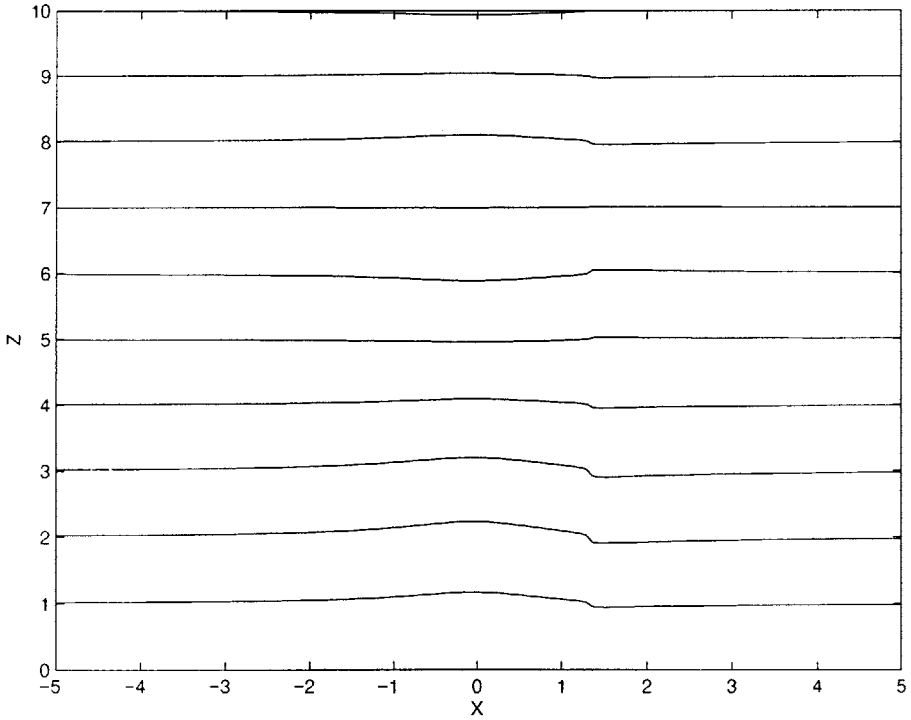

Figure 2.6: Flow with perturbation phase at 0.1625 radian.

Another remark on the critical phase is that it is unique for different BVF profiles. For example, when the stratified fluid has a unit BVF, the critical phase is 0, not at 0.13255 radian. On top of that, the critical phase does not exist for every BVF profiles. The existence of the critical phase is on the case-by-case basis.

2.2.3 Effects of background perturbation on wave breaking

Periodic disturbance on the BVF can cause wave to 'prematurely' break, as the previous section has shown. It can also cause wave not to break until the topography height is larger than 0.85. Figure 2.9 gives the visual confirmation that the wave breaking occurs when the topography is at 0.85. Figure 2.10, shows the same flow but with a periodic disturbance. For the latter case, the wave starts breaking only when the topography is at 1. In the simulation, the disturbance amplitude is set to 0.1 and its phase is set to $\pi/2$.

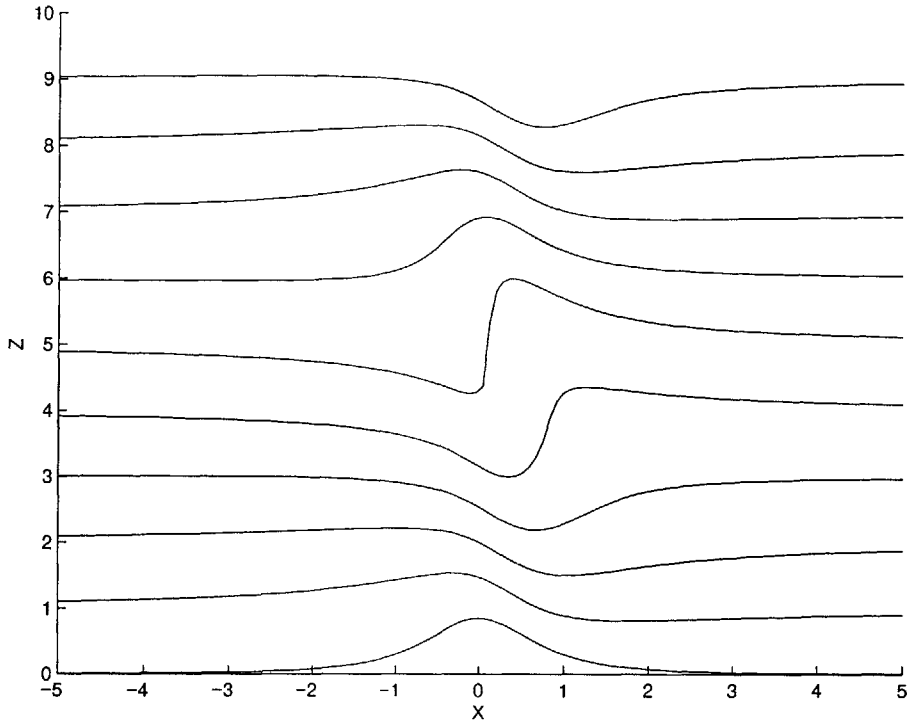

Figure 2.7: Flow with uniform BVF, no perturbation and with topography height at 0.85.

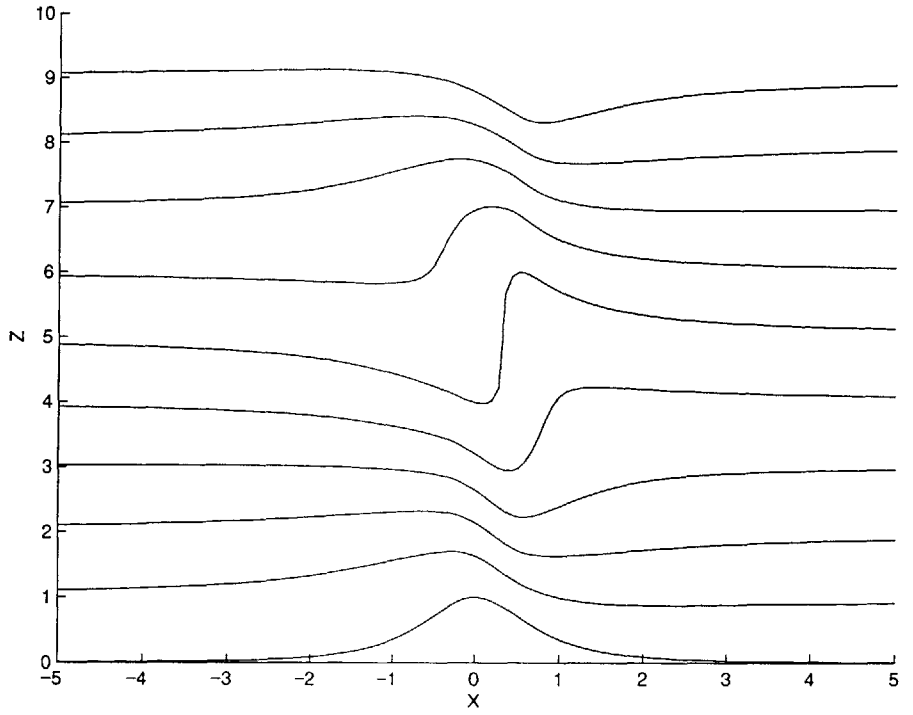

Figure 2.8: Flow with the periodically disturbed uniform BVF at topography of 1.

Chapter Three

Three dimensional stratified flow

Striving to achieve a better model of the stratified fluid flow over topography, the logical next step is to do a three-dimensional flow model. In this section, numerical simulations will be carried out to examine the effect of the periodic disturbance for three-dimensional flows. A non-linear three-dimensional analysis is beyond the scope of this thesis. Section 3.1 presents the general theory of the three-dimensional small-amplitude stratified flow. Section 3.2 discusses the results of the numerical simulations

3.1 Theory

Similar to the two dimensional case, the governing equations of the three-dimensional case begins with the conservation of mass and momentum equations.

$$\nabla \cdot \vec{u} = 0 \tag{3.1}$$

$$\vec{u} \cdot \nabla \rho = 0 \tag{3.2}$$

$$\rho \vec{u} \cdot \nabla \rho = -\nabla p + \rho \vec{g} \tag{3.3}$$

The following streamfunction and vorticity will be used.

$$\vec{u} = \nabla \Psi \times \nabla \Phi \,,\ \vec{\omega} = \nabla \times \vec{u} \,. \tag{3.4}$$

These two relationships will help simplify calculation and make visualizing stratified fluid flow possible. The detail of the derivation is presented in section 3 of the appendix. The governing equation is reduced and made dimensionless below.

$$\psi_{xxzz} + N^2(z)\left(\psi_{xx} + \psi_{yy}\right) = 0 \tag{3.5}$$

There are two boundary conditions, the lower boundary conditions and the radiation condition. The lower boundary condition is expressed as

$$\Psi(x,y,z)_{z=f} = \text{arbitrary constant} \tag{3.6}$$

f is the topography and is defined as

$$f(x,y) = \frac{h}{\left[1+(x/L_x)^2+(y/L_y)^2\right]^{3/2}} \tag{3.7}$$

Equation 3.6 can also be expressed as equation 3.8 in the streamline perturbation form with the arbitrary constant sets to zero.

$$\psi(x,y,z)_{z=0} + f = 0 \tag{3.8}$$

The radiation condition states that wave energy must propagate away from the source. It cannot move toward the source. This condition requires the group velocity to be positive. Group velocity is the speed at which the energy travels. The dispersion relation of the stratified fluid in large depth is,

$$\varpi(k,l,m) = k - \frac{\mathrm{sgn}(k)\mathrm{sgn}(m)N\sqrt{k^2+l^2}}{m} \tag{3.9}$$

Using this dispersion relation, the group velocity is

$$c_{g,z} = \frac{\mathrm{sgn}(k)\mathrm{sgn}(m)N\sqrt{k^2+l^2}}{m^2} \tag{3.10}$$

In order for the group velocity to be positive, the following condition must be true.

$$km > 0 \tag{3.11}$$

The solution to equation 3.5 can be obtained by using the Fourier transform. First, equation 4.5 is transformed into the frequency domain using equation 3.12 and a solution is obtained. Then, the solution is transformed back to the real domain.

$$\psi(x,y,z) = \int_{-\infty}^{\infty}\int_{-\infty}^{\infty}\hat{\psi}(k,l,z)e^{i(kx+ly)}dkdl \tag{3.12}$$

The transformed governing equation is,

$$\hat{\psi}_{zz} + m^2\hat{\psi} = 0 \tag{3.13}$$

$$m = N\frac{\sqrt{k^2 + l^2}}{k} \tag{3.14}$$

k and l are the horizontal wave numbers. The solution to the governing equation 3.13 is

$$\hat{\psi}_1(k,l,z) = A(k,l)\eta_1(z) + B(k,l)\eta_2(z) \tag{3.15}$$

η_1 and η_2 are obtained by integrating of the following differential.

$$\frac{d^2\eta}{dz^2} + m^2(z)\eta(z) = 0 \tag{3.16}$$

$$\eta_1(0) = 1,\ \frac{d\eta_1}{dz}(0) = 0\ \ \eta_2(0) = 0\ \frac{d\eta_2}{dz}(0) = 1 \tag{3.17}$$

The coefficients, A and B, of equation 3.15 are found using the lower boundary condition and the radiation condition. First step is to realize the solution far away the topography where the BVF is constant can be represented by

$$\hat{\psi}_2 = Ce^{im_\infty(z_\infty)} + De^{-im_\infty(z_\infty)} \tag{3.18}$$

Equation 3.15 must match equation 3.18 at a height when the BVF becomes constant. This condition is expressed in the following two equations.

$$\hat{\psi}_1(k,l,z_\infty) = \hat{\psi}_2(k,l,z_\infty) \tag{3.19}$$

$$\frac{\partial\hat{\psi}_1}{\partial z}(k,l,z_\infty) = \frac{\partial\hat{\psi}_2}{\partial z}(k,l,z_\infty) \tag{3.20}$$

Equations 3.19 and 3.20 say that the wave displacement and wave speed must be matched between the two solutions. Combining equations 3.8, 3.11, 3.15, and 3.18 together with equation 3.19 and 3.20 will setup a relationship between the four coefficients (A, B, C, and D). First of all, coefficient D is set to zero because of the radiation condition requiring that all wave number m and k to have the same sign. Since the vertical wave

number associated with the coefficient D is negative in equation 4.18 while wave number k is positive, D must be zero to satisfy the radiation condition. The lower boundary condition gives,

$$A(k,l) = -f \tag{3.21}$$

After finding A and D, coefficient B is determined to be,

$$B(k,l) = \left. \frac{\eta_{1z} - im_{\infty}\eta_1}{\eta_{2z} - im_{\infty}\eta_2} \right|_{z=z_{\infty}} \hat{f} \tag{3.22}$$

Substituting equation 3.21 and 3.22 into equation 3.15 completes the solution of the governing equation, equation 3.5, in the frequency domain. Then, it is transformed back to the real domain.

Equation 3.14 presents a problem for the numerical simulation because it is not defined when k equals to zero. The problem can be solved in a couple of ways. The most efficient method is to set the solution of the governing equation equal to zero when k equals to zero. This method allows the implementation of the traditional FFT method in transforming the solution back to the real domain.

3.2 Discussion

In this section, numerical simulations are performed to investigate the effect of the periodic disturbance on the three-dimensional stratified flow and its results are discussed.

3.2.1 Flow with uniform BVF.

Figure 3.1 shows a three-dimensional stratified flow with a unit BVF over topography. The flow consists of fluid going over the top and around the topography. Flow pattern has been studied by Durran (1992). The flow compares well with the flow Smith (1980) simulated. A nice three-dimensional plot of his simulated flow can be found in Baines (1995).

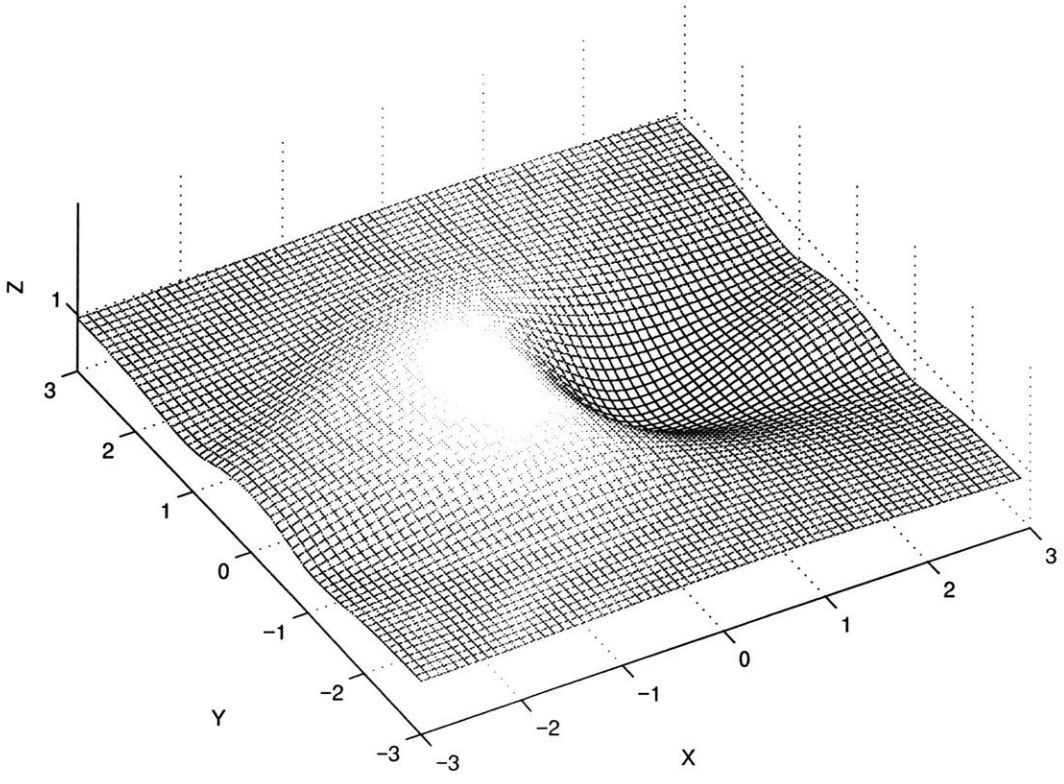

Figure 3.1: 3D uniform stratified flow.

Figure 3.2 shows two sets of streamlines projected onto the plane perpendicular to the y-axis slicing through the center of the flow in figure 3.1. It compares the wave activity for the flow going over a round topography and the flow going over a large spanwise topography. The comparison points out that wave activity is much smaller for flow going over the round topography.

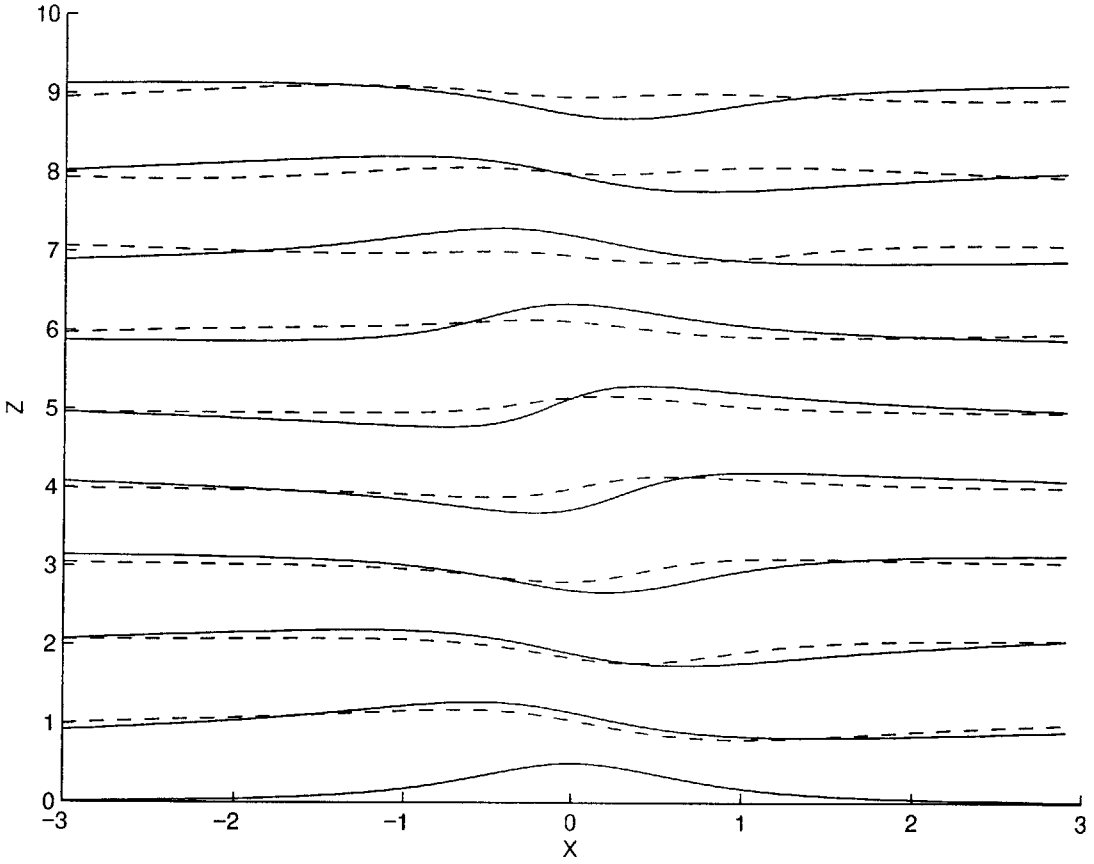

Figure 3.2: Comparison of flows over round topography and 1/16 topography.

The solid line represents fluid flowing over topography with the aspect ratio of 1 to 16. The length of the topography in the spanwise direction is 16 times longer than its length in the flow direction. The dotted line represents flow over round topography. The topography height in both cases is set to 0.5. The large difference observed between the

two flows can be attributed to the shape of the topography. The round topography naturally has less area of protrusion than the rectangular topography. Therefore, less fluid gets excited in the former case.

3.2.2 Effects of periodic disturbance in BVF on three-dimensional stratified flow

Figure 3.3 shows stratified flow with periodically perturbed uniform BVF. In the simulation, the disturbance amplitude is set to 0.2 and its phase equals to $\pi/2$.

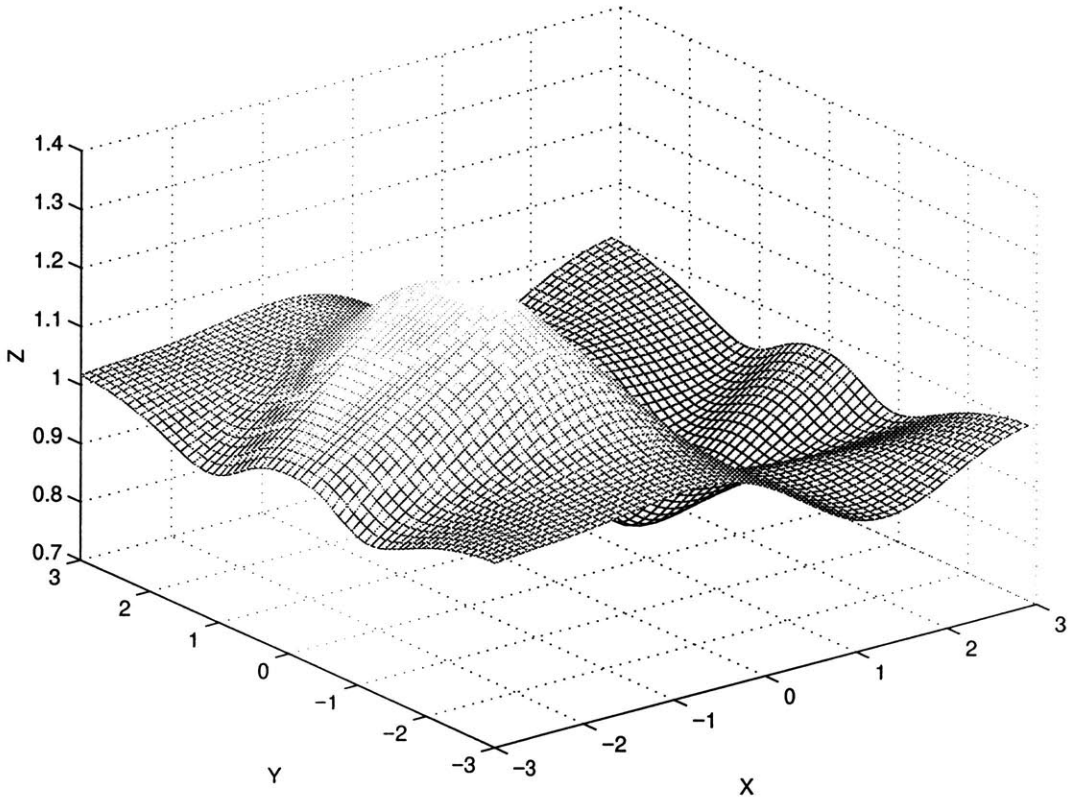

Figure 3.3: Flow with periodically perturbed uniform BVF.

Figure 3.3 shows that there are distinct differences for the flow with the perturbation and for the flow without the perturbation. In the case with the disturbance, there are depressions to the right and left in the downstream region of the flow. However, the main flow component remains the similar in both flows.

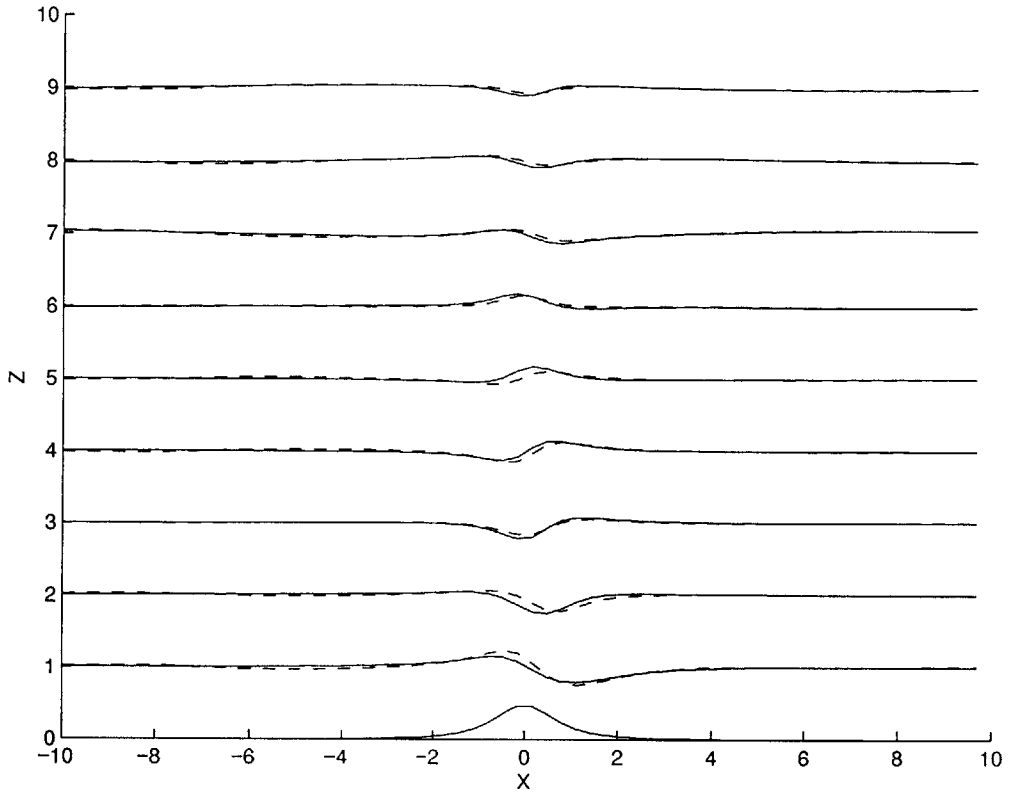

Figure 3.4: Comparison between flow with perturbation and with perturbation for flow over round topography.

Figure 3.4 shows stratified flows with the disturbance and without the disturbance over a round topography. The figure shows the streamlines on the plane cutting through the centerline. The solid line represents the flow without the disturbance to its BVF. The dotted line represents flows with the disturbance. From looking at the plot, both sets of flows look almost alike. This suggests that the periodic disturbance has little impact on the flow when the topography is round.

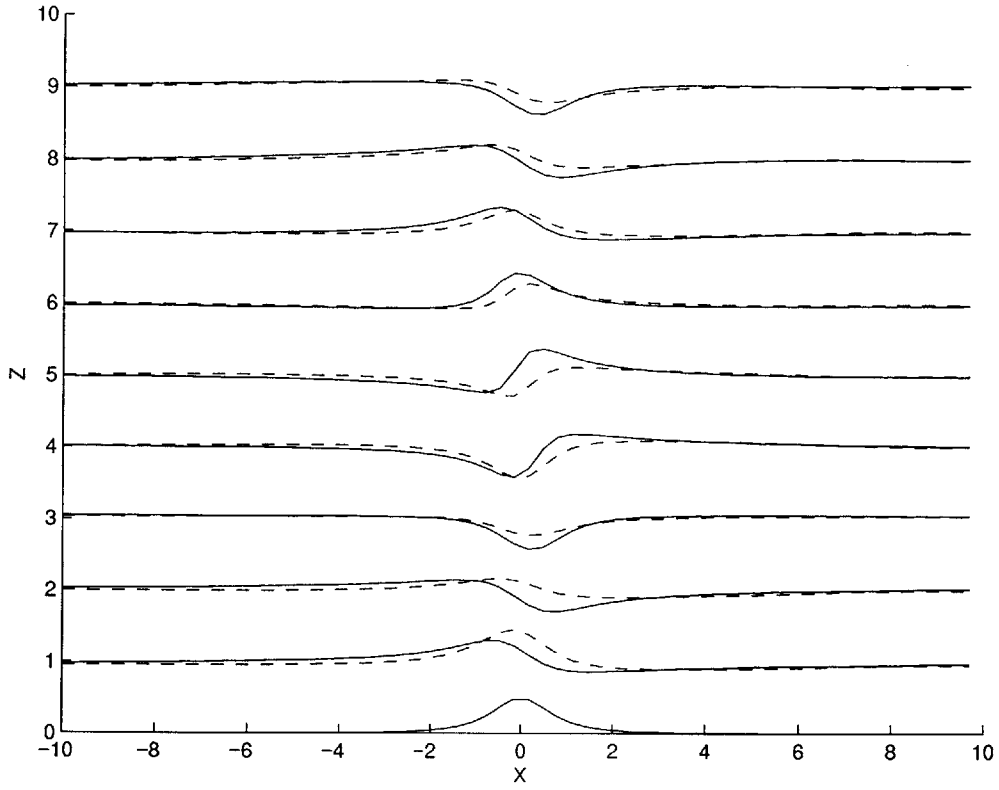

Figure 3.5: Comparison between flow with perturbation (dotted lines) and without perturbation (solid lines) for flow over 1/16 topography.

Figure 3.5 shows two sets of stratified fluid flow over large spanwise mountain. The solid streamlines represent the flow without any disturbance to its BVF. The dotted streamlines represent the flow with the disturbance to its BVF. The flow with the disturbance shows that its wave activity decreases as it propagates further away from the topography. In contrast, the wave activity for the flow without the disturbance does not change.

The observable difference between the two sets of flow shows that periodic disturbance has more influence on flow going over a large spanwise topography than on flow going over a round topography.

3.2.3 Flow with unstable phase

Numerical results in section 2.2.3 show the existence of a critical phase in two-dimensional stratified flow. At critical phase or phase close to it, the flow becomes unstable. This section does an investigation on the effect of the critical phase on the three-dimensional stratified flow. Previously in two-dimensional analysis, the flow with the following BVF profile was unstable when the perturbation phase is close to 0.13255 radian.

$$a = 1;\ b = 1/3;\ c = 20;\ d = 5$$

In the investigation of the critical phase in the three-dimensional flow, the same BVF profile described above is used and the critical phase remains the same. Numerical simulation is performed on two cases. In the first case, the flow is simulated going over a round topography and the resulting streamlines are plotted in Figure 3.6. The solid streamlines represent the flow with the disturbance phase equal to $\pi/2$ radian. The dotted streamlines represent the flow with the disturbance phase at 0.13255 radian. In the second case, the flow is simulated going over a large spanwise topography and it is plotted in Figure 3.7. Like in the first case, the solid streamlines represent the flow with the disturbance phase at $\pi/2$ radian and the dotted streamlines represent the flow with the disturbance phase at 0.13255 radian.

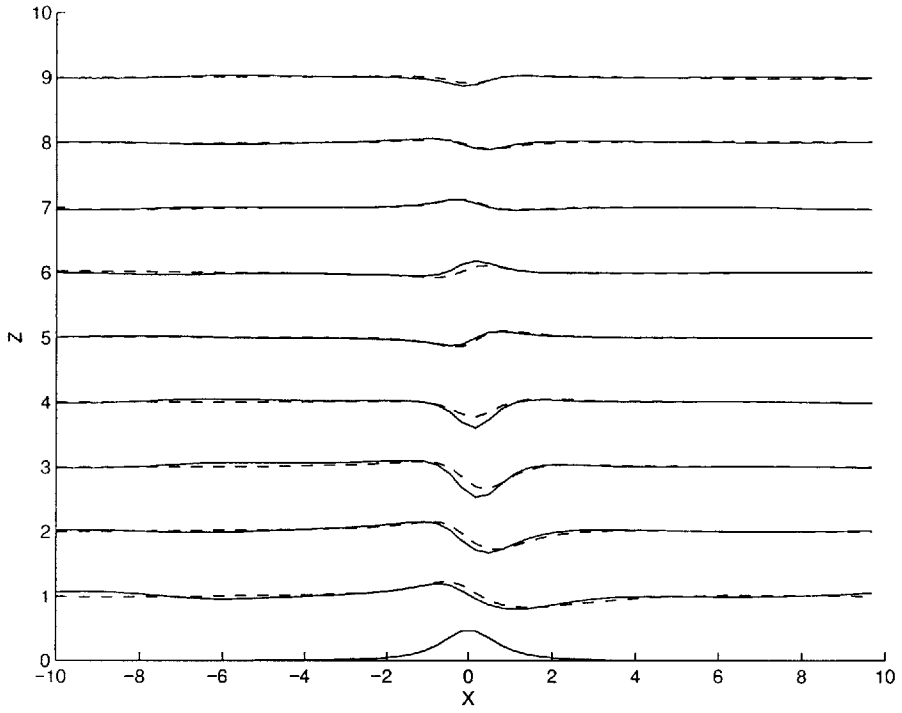

Figure 3.6: Comparison between the flow with disturbance phase at $\pi/2$ radian and phase at 0.13255radian over round topography.

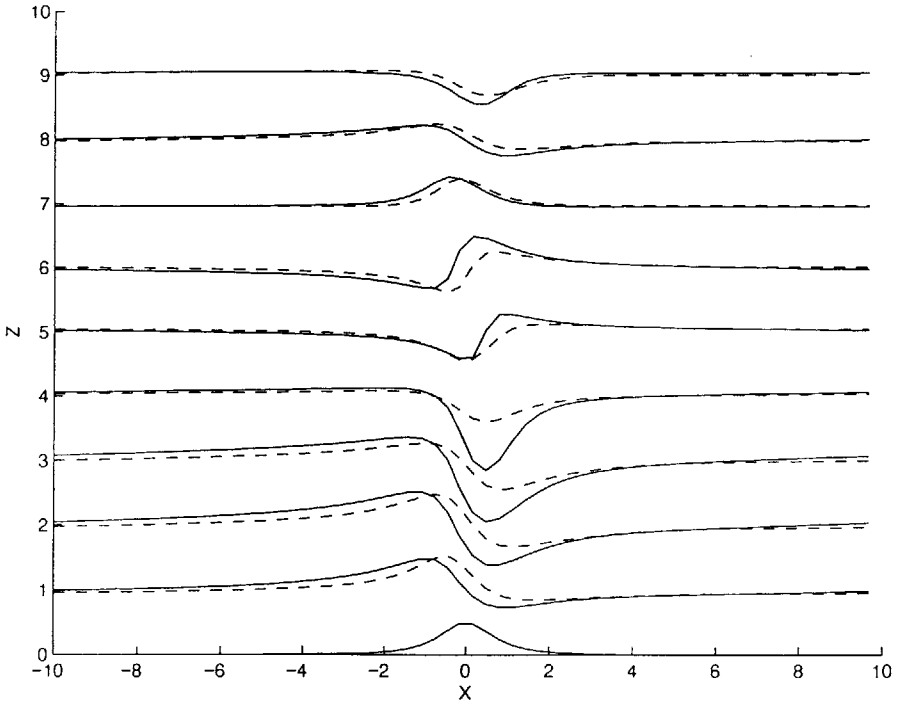

Figure 3.7: Comparison between the flow with disturbance phase at $\pi/2$ radian and phase at 0.13255radian over 1/16 topography.

As expected, the periodic disturbance does not have much influence on the flow going over a round topography. However, when the flow is going over a large spanwise topography, Figure 3.7 shows that the disturbance is a big factor and, hence, the critical phase has large effect.

The last comment in this section is that the two dimensional analysis predicted that the stratified flow would have become unstable before the disturbance phase reaches the critical value. However, the three-dimensional analysis shows that the flow remains stable and when it flows over a large spanwise topography, it showes that wave activity increases significantly.

Chapter Four

Analysis of data from the Air Force

A set of data on airflow over topography was received from the Air Force. This raw data will be analyzed for the purpose of exploring the effect of the tropopause on the induced gravity waves. The data describes airflow over mountains in the region from latitude 31.5N to 36N and longitude 104.5W to 110W. The terrain contour plot is given in Figure A.2. The mountain range in this region has a large transverse dimension in the north-south direction. If the air flows across the mountain in a perpendicular fashion, the flow can be modeled as two-dimensional.

The numerical simulation will use the data as a guide. The important variables from the data are the terrain contour, the tropopause height, the wind velocity profiles, and the BVF profile. These quantities are plotted in the appendix.

The x-direction and y-direction wind speed varied vertically from 0 m/s to upward of 30 m/s and from –5 m/s to 10 m/s, respectively; x-direction refers to the longitudinal direction and y-direction refers to the latitudinal direction. This condition approximates a two-dimensional flow because one component of the wind velocity is relatively small and the mountain range is long in the spanwise direction. In addition, the wind fluctuates at low altitude while at higher altitude outside the boundary layer, the velocity has a more uniform profile. At an even higher altitude, the wind speed is reduced back to the undisturbed value. Figure A.1 shows a typical looking velocity profile just described.

Figure A.2 shows the observed tropopause height, ranging from around 10km to upward of 15km. This quantity will be important later. The BVF (Brunt-Vaisala frequency) profiles at different locations of the terrain are plotted in Figures A.3, A.4 A.5

and A.6. These locations are selected to emphasize the wave activity in relation to the tropopause height. The square of the BVF profile is shown in the plots. It has a typical value of 0.0001 to 0.0005 [1/sec^2].

It should be noted that the BVF and velocity profiles include both the 'ambient' value and perturbations due to the induced gravity waves. Therefore, any increase in wave activity will be apparent in both of these profiles. The velocity profiles are plotted together with the BVF profiles in Figures A.3, A.4, A.5, and A.6.

4.1 Numerical simulation

The simulated flow will be modeled, within the limitations of the theory, based on the actual flow described in the last section. In the simulation, the incoming flow will have a uniform profile with a value characteristic of the actual wind velocity profile. Figure A.1 shows a typical wind velocity profile.

Also, the simulation will use a model of a typical looking BVF profile. A typical BVF profile approximately consists of two layers of constant BVF. The lower layer usually has a smaller BVF than the upper layer. A hyperbolic tangent is used to represent this BVF profile.

In addition to the assumptions mentioned above, the simulation assumes the flow is inviscid, incompressible, and steady. Also, the hydrostatic approximation and the Boussinesq approximation are made.

The simulation will use the following non-linear governing equation for the streamfunction perturbation ψ:

$$\psi_{zz} + N^2(\psi + z)\psi = 0,$$

where N is the BVF profile. The two boundary conditions are the lower boundary and the radiation condition. The lower boundary states that the flow has to conform to the topography. The radiation condition states that the wave energy must propagate away from the source.

The values used in the simulation are the following. The incoming velocity has a magnitude of about 30m/s. The BVF has one value in the lower layer and another in the upper layer: 0.01 [1/sec] and 0.025 [1/sec], respectively. As mentioned earlier, the BVF

profile is described by the hyperbolic tangent function. Also the peak mountain height used for the simulation is 1800m, consistent with the terrain shown in Figure A.2.

In previous works, the tropopause height was found to be an influencing factor: the induced wave disturbance becomes more active at certain tropopause heights. This is the motivation for the present numerical simulation and comparison of the simulated results with the data. To study the effects of the tropopause height, numerical simulation is performed by varying the location of the tropopause and observing how the wave activity changes.

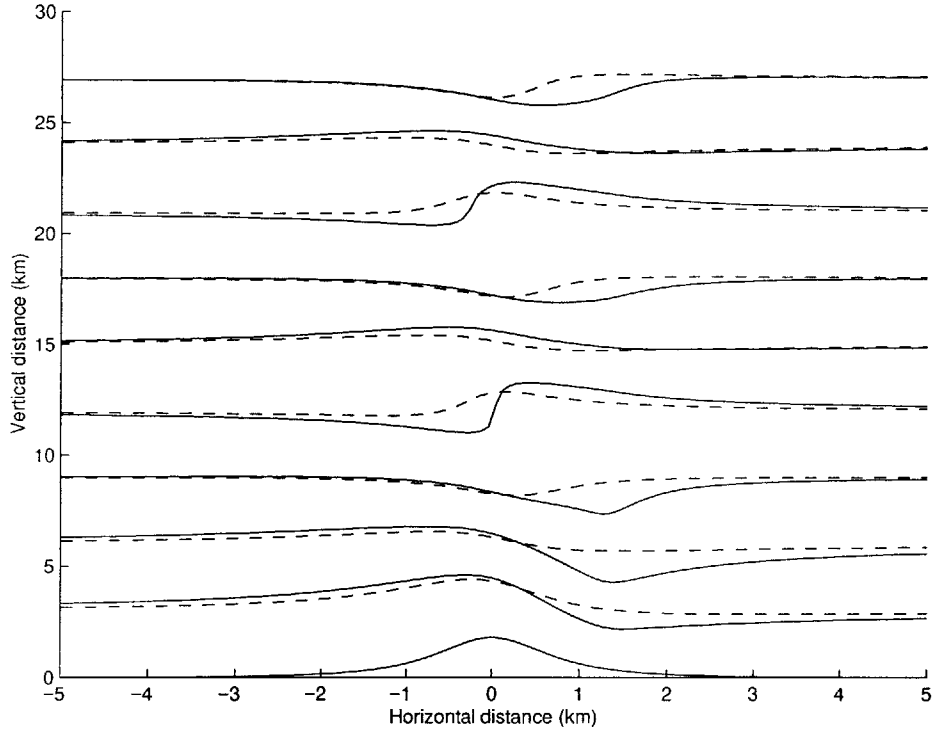

Figure 4.1: Simulated streamlines for two different tropopause heights.

Figure 4.1 shows streamlines corresponding to two different tropopause heights. Note that the wave activity is a function of the tropopause height as previously discovered. The solid streamline represents the flow with the tropopause height at 10.3km. The dotted streamline represents the flow at a lower tropopause height. From

looking at the plots, it is clear that the wave is more active when the tropopause height is at 10.3km. Figure 4.2 shows a more complete picture of the wave activity as a function of the tropopause height. Figure 4.2 is based on the second streamline in Figure 4.1. Specifically, a measure of wave perturbation is obtained by summing the squares of vertical displacement of this streamline at the computational grid points, and taking the square root; if there were no disturbance, this 'average' vertical streamline displacement would be zero. Flows with the tropopause height below 10km and above 15km have reduced wave activity. However, when the tropopause is between 10.5km to 14km, the simulation shows wave breaking and large wave activity (the missing section of the curve in Figure 4.2 is when the simulation predicts wave breaking).

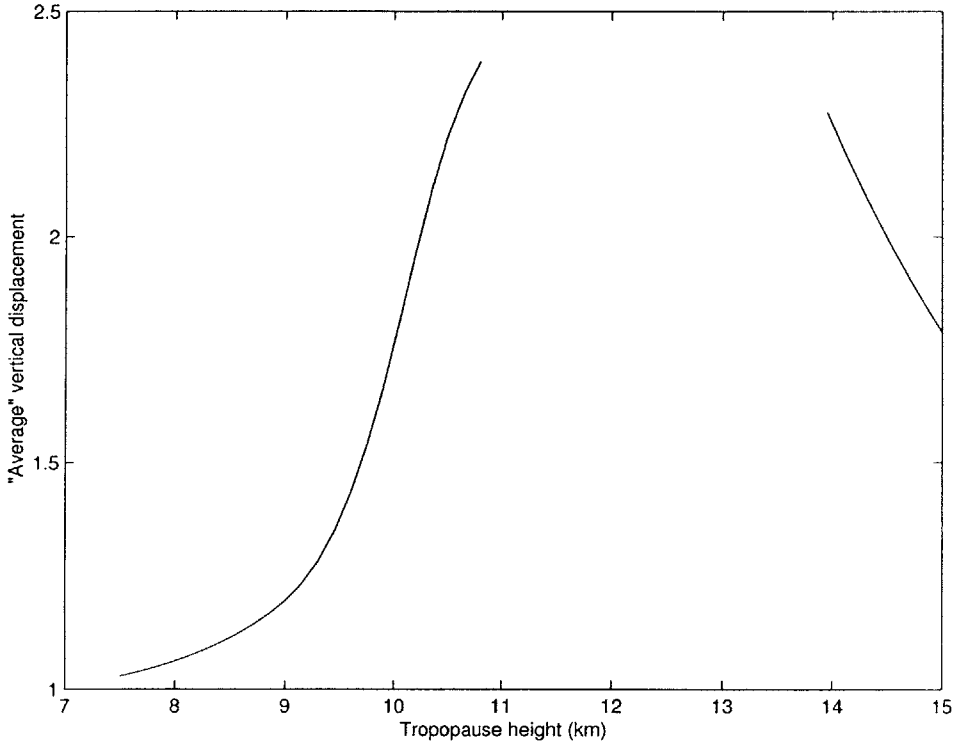

Figure 4.2: 'Average' vertical displacement of streamline at height 6km versus tropopause height.[1]

[1] Breaking occurs when the tropopause height is in the range of 10.5-13.5km.

Figure 4.3 shows a similar plot based on the streamline at 21km. The results are very similar to those in Figure 4.2.

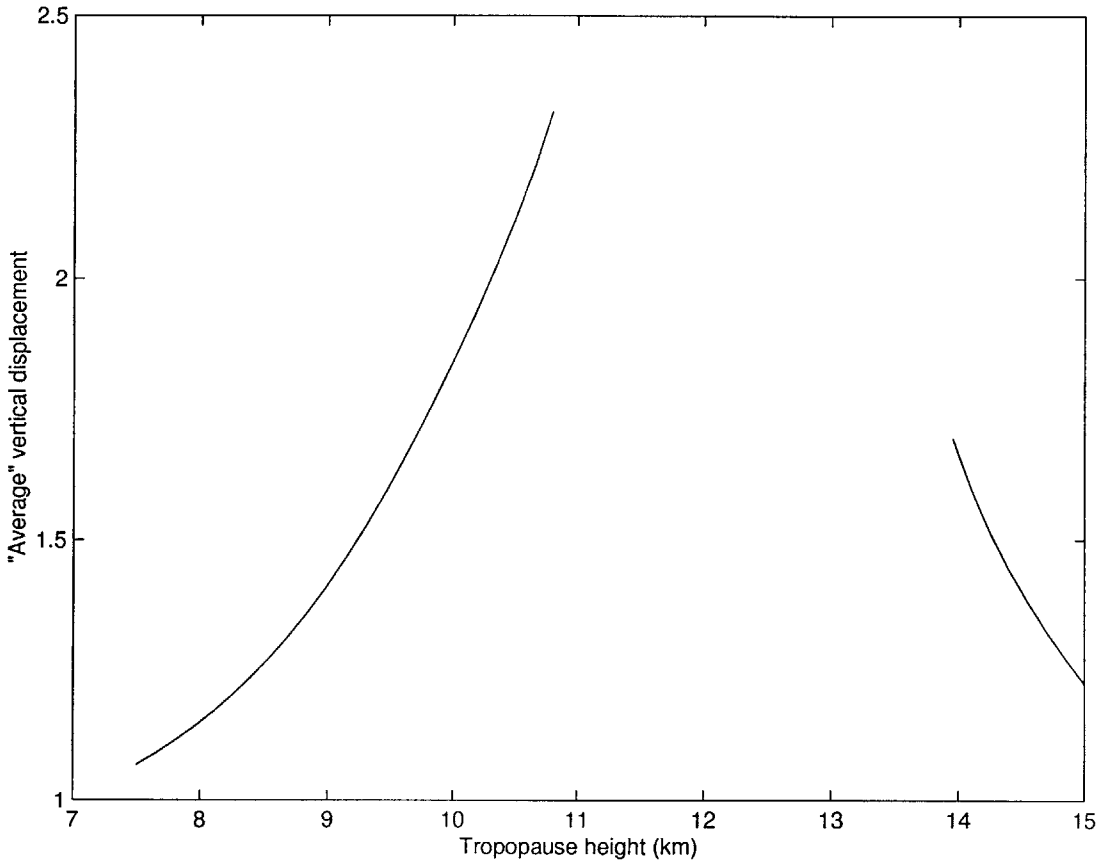

Figure 4.3: 'Average' vertical displacement of streamline at height 21km versus tropopause height.[2]

[2] Breaking occurs when the tropopause height is in the range of 10.5-13.5km.

4.2 Discussion

The numerical simulation suggests that tropopause heights between 10km to 14km can have a big influence on the generated wave. Furthermore, these tropopause heights are realizable. Figures A.5 and A.6 refer to the airflow with the tropopause around 10km to 11km. Figures A.3 and A.4 refer to the airflow with the tropopause around 15km to 16km. A closer look at the actual flow data shows that there is a significant wave activity when the tropopause height is between 10km to 11km. When the tropopause height reaches 15km to 16km, the data shows that the wave amplitude tapers down significantly. Specifically in Figure 4.4, we plot the disturbance amplitude of the BVF as a function of the tropopause height (this plot was constructed in a similar fashion to those in Figures 4.2 and 4.3 earlier, by considering deviations of the BVF from a 'mean' profile). Note that the wave activity is significantly more pronounced when the tropopause height is at 10-11km than when it is at 15-16km.

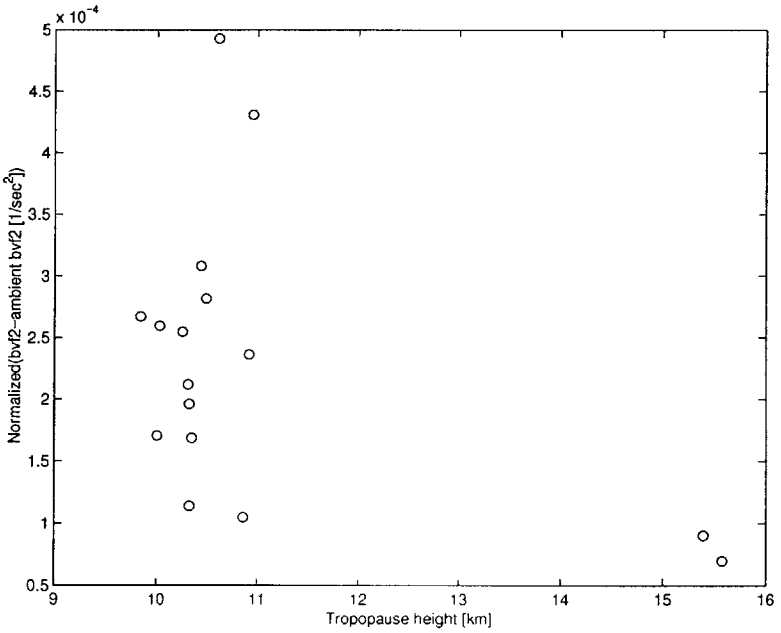

Figure 4.4: Disturbance amplitude of BVF from the data versus tropopause height.

The effects of the tropopause height on wave activity can also be seen from looking at the wind-velocity profiles. These profiles are plotted alongside the BVF profiles in Figures A.3, A.4, A.5, and A.6. When the tropopause height is such that it causes significant disturbances in BVF, the velocity profile also shows significant fluctuation. This is apparent in Figures A.5 and A.6.

The results from the numerical simulation in the previous section can help us to understand why at tropopause heights 15-16 km one should expect the generated mountain wave activity to be reduced. The incoming velocity in the simulation was assumed to be 30m/s and a nominal BVF of 0.01[1/sec] was used. For these values, the simulation shows that the tropopause height is tuned in the range 10.5-14km, as seen earlier. If the incoming velocity is taken as 10 m/s, on the other hand, the simulation suggests that the tuned tropopause height is 3km-5 km. In the actual flow, there is no tropopause at such low height and no large disturbances are found in the region where the incoming velocity is around 10m/s. Likewise, if the incoming velocity is increased to 45 m/s, the simulation predicts that the tuned tropopause height is 16km-22km. In the actual flow data, the wind speed never reached 45m/s so no large wave activity is to be expected when the tropopause height is above 16km or so. For the tropopause at around 10.5km to be tuned, the simulation suggests that the incoming velocity has to be 25m/s - 30m/s. In the actual flow, the incoming velocity indeed reaches 30 m/s between the heights of 10 to 30km (see figure A.1). This could explain why under those conditions, wave activity increases noticeably.

REFERENCES

BAINES, P. G. 1995. *Topographic effects in stratified flows*. Cambridge University Press, New York

DAVIS, K. 1999. Flow of Nonuniformly Stratified fluid of Large Depth over Topography. S.M. Thesis, MIT..

DURRAN, D.R. 1992. Two-Layer solutions to Long's equation for vertically propagating mountain waves: how good is linear theory? *Q.J.R. Meteorol. Soc.* **118**, 415.

KANTZIOS, Y. D. & AKYLAS, T. R. An asymptotic theory of nonlinear stratified flow of large depth over topography. *The Royal Society.* **440**, 639-653.

KLEMP, J. B. & LILLY, D. K. 1975. The dynamics of wave-induced downslope winds. *J. Atmos. Sci.* **32**, 320.

PHILLIPS, O. M. 1968. The interaction trapping of internal gravity waves. *J. Fluid Mech.* **34**, 407-416.

SMITH R. B. 1980. Linear theory of stratified hydrostatic flow past an isolated mountain. *Tellus*. **32**, 348-364.

APPENDIX

A.1 Two-dimensional stratified flow governing equation

The governing equations for the two-dimensional stratified fluid flow are

$$u_x + w_z = 0 \tag{A.1.1}$$
$$u\rho_x + w\rho_z = 0 \tag{A.1.2}$$
$$\rho(uu_x + wu_z) = -p_x \tag{A.1.3}$$
$$\rho(uw_x + ww_z) = -p_z - \rho g \tag{A.1.4}$$

Using the following dimensionless variables,

$$x = L\tilde{x},\ z = \frac{U_o}{N_o}\tilde{z},\ u = U_o\tilde{u},\ w = \frac{U_o^2}{LN_o}\tilde{w},\ \rho = \rho_o\tilde{\rho},\ p = \frac{gU_o\rho_o}{N_o}\tilde{p}$$

the dimensionless governing equations are

$$u_x + w_z = 0 \tag{A.1.5}$$
$$u\rho_x + w\rho_z = 0 \tag{A.1.6}$$
$$\beta\rho(uu_x + wu_z) = -p_x \tag{A.1.7}$$
$$\beta\rho(uw_x + ww_z) = -\mu^{-2}(p_z + \rho). \tag{A.1.8}$$

The β and μ terms are defined below.

$$\beta = \frac{N_o U_o}{g},\ \mu = \frac{U_o}{N_o L} \tag{A.1.9}$$

Using the following streamfunction,

$$u = \Psi_z,\ w = -\Psi_x \tag{A.1.10}$$

the governing equations are transformed to

$$\Psi_z\rho_x - \Psi_x\rho_z = 0 \tag{A.1.11}$$
$$\beta\rho(\Psi_z\Psi_{zx} - \Psi_x\Psi_{zz}) = -p_x \tag{A.1.12}$$
$$\beta\rho(-\Psi_z\Psi_{xx} + \Psi_x\Psi_{xz}) = -\mu^{-2}(p_z + \rho). \tag{A.1.13}$$

Eliminating the pressure term in equation A.1.12 and A.1.13 and combine them, the resulting equation becomes

$$\rho_z\left(\Psi_z\Psi_{zx}-\Psi_x\Psi_{zz}\right)+\rho\left(\Psi_z\Psi_{zx}-\Psi_x\Psi_{zz}\right)_z$$
$$+\mu^2\rho_x\left(\Psi_z\Psi_{xx}-\Psi_x\Psi_{xz}\right)+\mu^2\rho\left(\Psi_z\Psi_{xx}-\Psi_x\Psi_{xz}\right)_x-\frac{\rho_x}{\beta}=0. \qquad \text{(A.1.14)}$$

This equation is simplified by using the Jacobian defined below.

$$J\{A,B\}\equiv A_xB_z-A_zB_x \qquad \text{(A.1.15)}$$

The resulting equation is

$$\rho J\left\{\Psi_{zz}+\mu^2\Psi_{xx},\Psi\right\}+\frac{\rho_\Psi}{\beta\rho}J\left\{z+\frac{\beta}{2}\left(\Psi_z^2+\mu^2\Psi_x^2\right),\Psi\right\}=0 \qquad \text{(A.1.16)}$$

The dimensionless BVF is defined below.

$$N^2(\Psi)=-\frac{\rho_\Psi}{\beta\rho} \qquad \text{(A.1.17)}$$

Equation A.1.16 is further simplified to

$$J\left\{\Psi_{zz}+\mu^2\Psi_{xx}-N^2(\Psi)\left[z+\frac{\beta}{2}\left(\Psi_z^2+\mu^2\Psi_x^2\right)\right],\Psi\right\}=0 \qquad \text{(A.1.18)}$$

Integrating it gives

$$\Psi_{zz}+\mu^2\Psi_{xx}-N^2(\Psi)\left[z+\frac{\beta}{2}\left(\Psi_z^2+\mu^2\Psi_x^2\right)\right]=G(\Psi) \qquad \text{(A.1.19)}$$

The constant of integration 'G' is

$$G(\Psi)=-N^2(\Psi)\left(\Psi+\frac{\beta}{2}\right) \qquad \text{(A.1.20)}$$

The boundary conditions used to obtain A.1.20 are no upstream influence and the fluid density is a function of the streamline. After some simple manipulations, the resulting governing equation is

$$\Psi_{zz}+N^2(\Psi)(z-\Psi)+\mu^2\Psi_{xx}+\frac{\beta}{2}N^2(\Psi)\left(\Psi_z^2+\mu^2\Psi_x^2-1\right)=0.$$

By using hydrostatic and Bossinesq approximations, the β and μ drop out and the governing equation reduces to

$$\Psi_{zz} + N^2(\Psi)(\Psi - z) = 0 \qquad \text{(A.1.21)}$$

$\Psi = \psi + z$ is the streamfunction defined in equation A.1.10. ψ is the perturbation streamfunction. In term of the ψ, the governing equation is

$$\psi_{zz} + N^2(\psi + z)\psi = 0 \qquad \text{(A.1.22)}$$

A.2 Multiple scale analysis for linear flow with periodic disturbance to its BVF

In section 2.1.3, the method of multiple scales was applied on small-amplitude stratified flow to investigate the resonance condition. This section provides the detail. The analysis begins by looking at the small-amplitude governing equation with the following BVF.

$$N = N_o + A_p \sin(Tz + \phi) \qquad \text{(A.2.1)}$$

The second term of the above expression is the periodic disturbance. For the case when T equals 0, N remains constant, N_o. The following analysis examines the case when T is not zero.

The small-amplitude governing equation with the condition described above is

$$\eta_{zz} + \left[N_o + A_p \sin(Tz + \phi)\right]^2 \eta = 0. \qquad \text{(A.2.2)}$$

The magnitude of A_p is of the order of ε. Expanding the BVF term gives

$$\eta_{zz} + \left[N_o^2 + 2A_p N_o \sin(Tz + \phi) + {A_p}^2 \sin^2(Tz + \phi)\right]\eta = 0. \qquad \text{(A.2.3)}$$

The solution to the equation A.2.3 is the following equation, neglecting the higher order terms.

$$\eta = \eta_o + \eta_1 + ... \qquad \text{(A.2.4)}$$

The zero order case is described by the following governing equation.

$O(1)$:

$$\eta_{ozz} + N_o^2 \eta_o = 0 \qquad \text{(A.2.5)}$$

$$\eta_o(0)=1 \tag{A.2.6}$$

$$\eta_{oz}(0)=0 \tag{A.2.7}$$

$$\eta_o = Ae^{iN_o z} + Be^{-iN_o z} \tag{A.2.8}$$

$$A+B=1 \tag{A.2.9}$$

$$iN_o A - iN_o B = 0 \tag{A.2.10}$$

$$A=B=\frac{1}{2} \tag{A.2.11}$$

$$\eta_o = \frac{e^{iN_o z}+e^{-iN_o z}}{2} = \cos N_o z \tag{A.2.12}$$

Equation A.2.12 is the solution to equation A.2.5. The analysis for the first order is given below.

$O(\varepsilon)$:

$$\eta_{1zz} + N_o^2\eta_1 = -2A_p \sin(Tz+\phi)\eta_o = -2A_p N_o \sin(Tz+\phi)\cos N_o z \tag{A.2.13}$$

$$\eta_{1zz} + N_o^2\eta_1 = -2A_p N_o[\sin(Tz+\phi+N_o z)+\sin(Tz+\phi-N_o z)] \tag{A.2.14}$$

$$\eta_1 = Ae^{iN_o z} + Be^{-iN_o z} + C\sin(Tz+\phi+N_o z)+D\sin(Tz+\phi-N_o z) \tag{A.2.15}$$

Equation A.2.15 is the solution to the differential equation A.2.14. The coefficients are found by applying the boundary conditions. The particular solution is found by substituting equation A.2.15 back into equation A.2.14. This will determine the coefficient of C and D. The following is the steps used in obtaining the coefficients.

$$\begin{aligned} &-(T+N_o)^2 C\sin(Tz+\phi+N_o z)-(T-N_o)^2 D\sin(Tz+\phi-N_o z) \\ &+CN_o^2\sin(Tz+\phi+N_o z)+DN_o^2\sin(Tz+\phi-N_o z) \\ &=-2A_p N_o\sin(Tz+\phi+N_o z)-2A_p N_o\sin(Tz+\phi-N_o z) \end{aligned} \tag{A.2.16}$$

The two resulting simultaneous equations are

$$-(T+N_o)^2 C + CN_o^2 = -2N_o A_p \tag{A.2.17}$$

$$-(T-N_o)^2 D + DN_o^2 = -2N_o A_p \tag{A.2.18}$$

Solving equation A.2.17 and A.2.18 for C and D gives

$$C = \frac{2N_o A_p}{(T+N_o)^2 - N_o^2} \tag{A.2.19}$$

$$D = \frac{2N_o A_p}{(T-N_o)^2 - N_o^2} \tag{A.2.20}$$

Then equation A.2.15 becomes

$$\begin{aligned}\eta_1 = {} & Ae^{iN_o z} + Be^{-iN_o z} + \frac{2N_o A_p}{(T+N_o)^2 - N_o^2}\sin(Tz+\phi+N_o z) \\ & + \frac{2N_o A_p}{(T-N_o)^2 - N_o^2}\sin(Tz+\phi-N_o z)\end{aligned} \tag{A.2.21}$$

A and B will be determined next by using the following two boundary conditions.

$$\eta_1(0) = 0 \tag{A.2.22}$$

$$\eta_{1z}(0) = 0 \tag{A.2.23}$$

The resulting equations from applying the boundary conditions are

$$0 = A + B + \left[\frac{2N_o A_p}{(T+N_o)^2 - N_o^2} + \frac{2N_o A_p}{(T-N_o)^2 - N_o^2}\right]\sin\phi \tag{A.2.24}$$

$$0 = iN_o A - iN_o B + \frac{2A_p N_o (T+N_o)}{(T+N_o)^2 - N_o^2}\cos\phi + \frac{2A_p N_o (T-N_o)}{(T-N_o)^2 - N_o^2}\cos\phi \tag{A.2.25}$$

Solving equation A.2.24 and A.2.25 determines the coefficients A and B.

$$B = \frac{F - iE}{2i} \tag{A.2.26}$$

$$A = \frac{-iE - F}{2i} \tag{A.2.27}$$

The variable E and F are defined below.

$$E = \left[\frac{2N_o A_p}{(T+N_o)^2 - N_o^2} + \frac{2N_o A_p}{(T-N_o)^2 - N_o^2} \right] \sin\phi \qquad \text{(A.2.28)}$$

$$F = \left[\frac{2A_p N_o (T+N_o)}{(T+N_o)^2 - N_o^2} + \frac{2A_p N_o (T-N_o)}{(T-N_o)^2 - N_o^2} \right] \cos\phi \qquad \text{(A.2.29)}$$

Finally, substituting equations A.2.26 and A.2.27 into equation A.2.21 gives the solution to the order ε differential equation.

$$\eta_1 = -\frac{iE+F}{2i} e^{iN_o z} + \frac{F-iE}{2i} e^{-iN_o z} + \frac{2N_o A_p}{(T+N_o)^2 - N_o^2} \sin(Tz + \phi + N_o z)$$

$$+ \frac{2N_o A_p}{(T-N_o)^2 - N_o^2} \sin(Tz + \phi - N_o z) \qquad \text{(A.2.30)}$$

The solution to the equation A.2.2 is the sum of equation A.2.12 and equation A.2.30.

A.3 Three-dimensional stratified fluid flow governing equation

Like in the two dimensional flow, the governing equations of the three-dimensional case begins with the conservation of mass and momentum equation.

$$\nabla \cdot \vec{u} = 0 \tag{A.3.1}$$

$$\vec{u} \cdot \nabla \rho = 0 \tag{A.3.2}$$

$$\rho \vec{u} \cdot \nabla \rho = -\nabla p + \rho \vec{g} \tag{A.3.3}$$

The first step in obtaining the solution is to introduce the streamfunction and vorticity, defined below.

$$\vec{u} = \nabla \Psi \times \nabla \Phi \,,\ \vec{\omega} = \nabla \times \vec{u} \,. \tag{A.3.4}$$

Beside the incompressible and inviscid assumptions used, this model also assumes there is no upstream influence. This means that the density is only a function of the height. The incoming velocity also is taken to have a uniform profile. They are expressed as

$$\vec{u} = U_o i \,,\ \rho = \rho_o(z) \tag{A.3.5}$$

Equation A.3.5, in terms of streamfunction, is

$$\Psi = U_o z \,,\ \Phi = y \tag{A.3.6}$$

$$\rho = \rho_o\left(\frac{\Psi}{U_o}\right) \tag{A.3.7}.$$

Using streamfunction and vorticity with some manipulations, the conservation of momentum equation is expressed as

$$\rho(\vec{\varpi} \times \vec{u}) = -\nabla\left(p + \frac{1}{2}\rho|\vec{u}|^2 + \rho \vec{g} z\right) + \nabla\rho\left(\frac{1}{2}|\vec{u}|^2 + \vec{g} z\right) \tag{A.3.8}$$

Vorticity theorem states that

$$\vec{\varpi} \cdot \nabla \Psi = 0 \qquad \text{(A.3.9)}$$

Using this fact, the left hand side of equation A.3.8 is transformed to,

$$\vec{\varpi} \times \vec{u} = (\vec{\varpi} \cdot \nabla \Phi) \nabla \Psi \qquad \text{(A.3.10)}$$

Applying the boundary conditions stated in equations A.3.6 and A.3.7, the conservation of momentum equation further simplify to

$$\vec{\varpi} \cdot \nabla \Phi = \frac{1}{\rho} \frac{d\rho}{d\Psi} \left[\frac{1}{2} U_0^2 - \frac{1}{2} |\vec{u}|^2 + \frac{g}{U_o} (\Psi - U_o z) \right]$$

The following dimensionless numbers are used to make the governing equation simpler.

$$x = L\tilde{x},\ y = L\tilde{y}, z = \frac{U_o}{N_o}\tilde{z},\ u = U_o\tilde{u},\ v = U_o\tilde{v}\ w = \frac{U_o^2}{LN_o}\tilde{w},\ \rho = \rho_o\tilde{\rho},$$

$$p = \frac{gU_o\rho_o}{N_o}\tilde{p}, \Psi = \frac{U_o^2}{N_o}\tilde{\Psi},\ \Phi = L\tilde{\Phi}$$

After using the streamfunction and the dimensionless number, the governing equations are transformed into

$$\vec{\varpi}_H \cdot \nabla \Phi + N^2(\Psi)(\Psi - z) = 0 \qquad \text{(A.3.11)}$$

$$\vec{\varpi}_H \cdot \nabla \Psi = 0 \qquad \text{(A.3.12)}$$

$$\vec{\varpi}_H = \left(-\frac{\partial v}{\partial z}, \frac{\partial u}{\partial z}, \frac{\partial v}{\partial x} - \frac{\partial u}{\partial y} \right) \qquad \text{(A.3.13)}$$

In terms of the streamline perturbation ($\Psi = \psi + z, \Phi = \phi + y$), equations A.3.11 and A.3.12 become

$$\psi_{zz} + N^2(z)\psi + \phi_{yz} = 0 \qquad \text{(A.3.14)}$$

$$\phi_{xx} + \phi_{yy} + \psi_{yz} = 0 \qquad \text{(A.3.15)}$$

Combining the previous two equations, the result is a three-dimensional stratified flow governing equation, in a dimensionless form.

$$\psi_{xxzz} + N^2(z)(\psi_{xx} + \psi_{yy}) = 0 \qquad \text{(A.3.16)}$$

A.4 Data from the Air Force

Each unit of height of the plots in this appendix represents 500m. All the profiles are plotted between 0km and 30km. The profile plots are figure A.1, A.3, A.4, A.5, and A.6. The units of these plots are as followed: the velocity is in [m/s] and the BVF2 is in [1/sec^2].

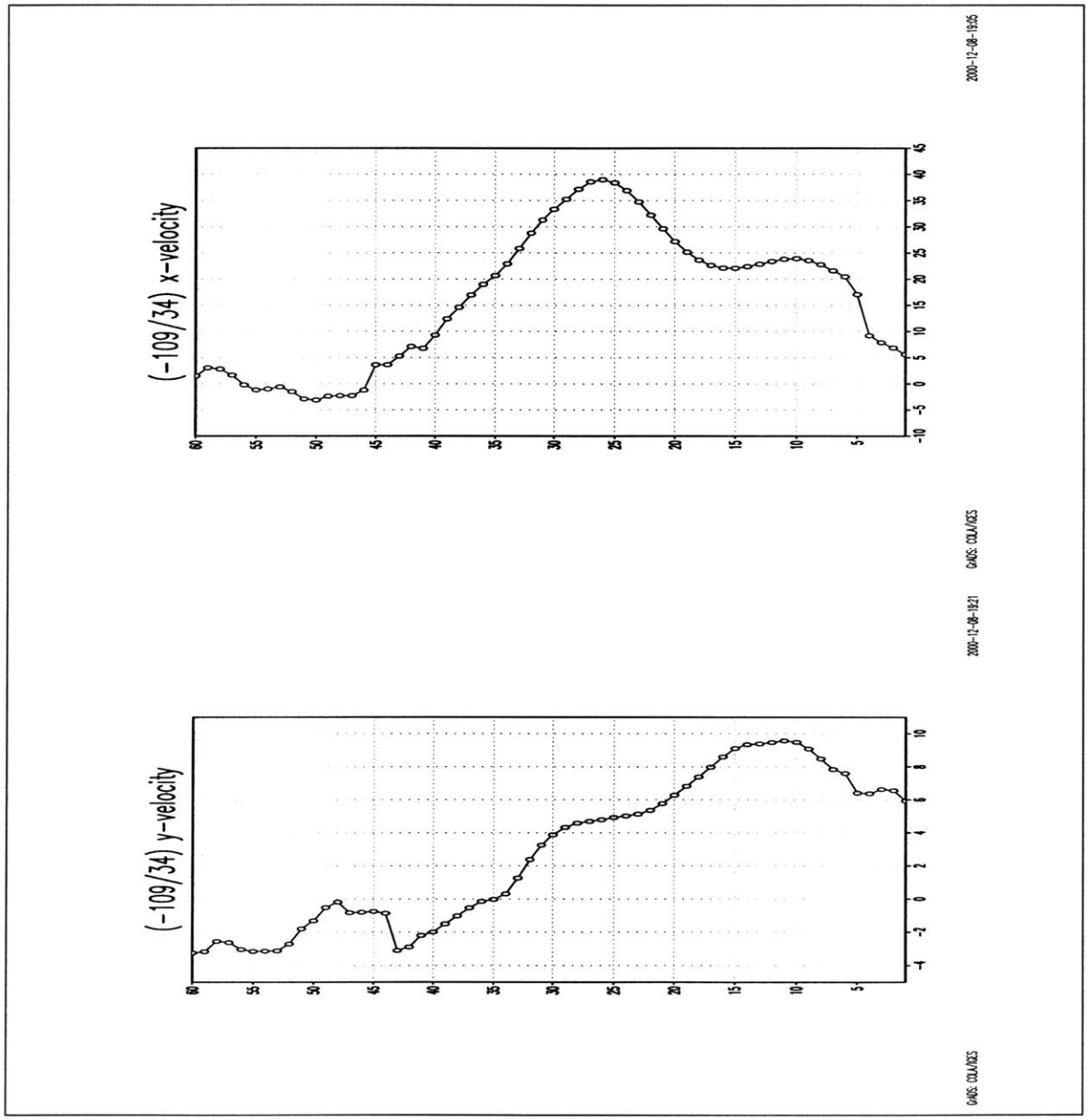

Figure A.1: Velocity profiles in the longitudinal (top) and latitudinal direction.

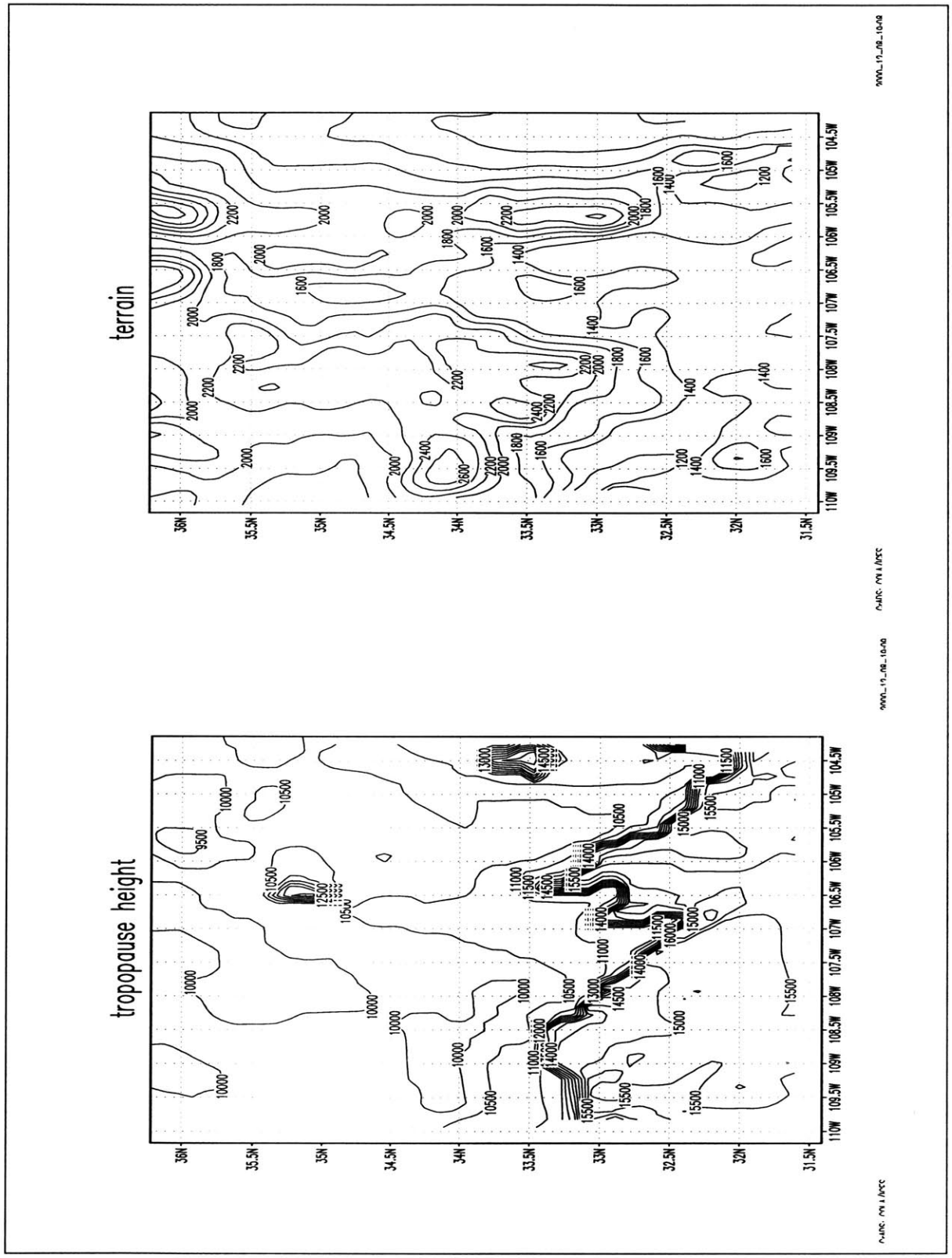

Figure A.2: Top plot: terrain contour. Bottom plot: tropopause contour.

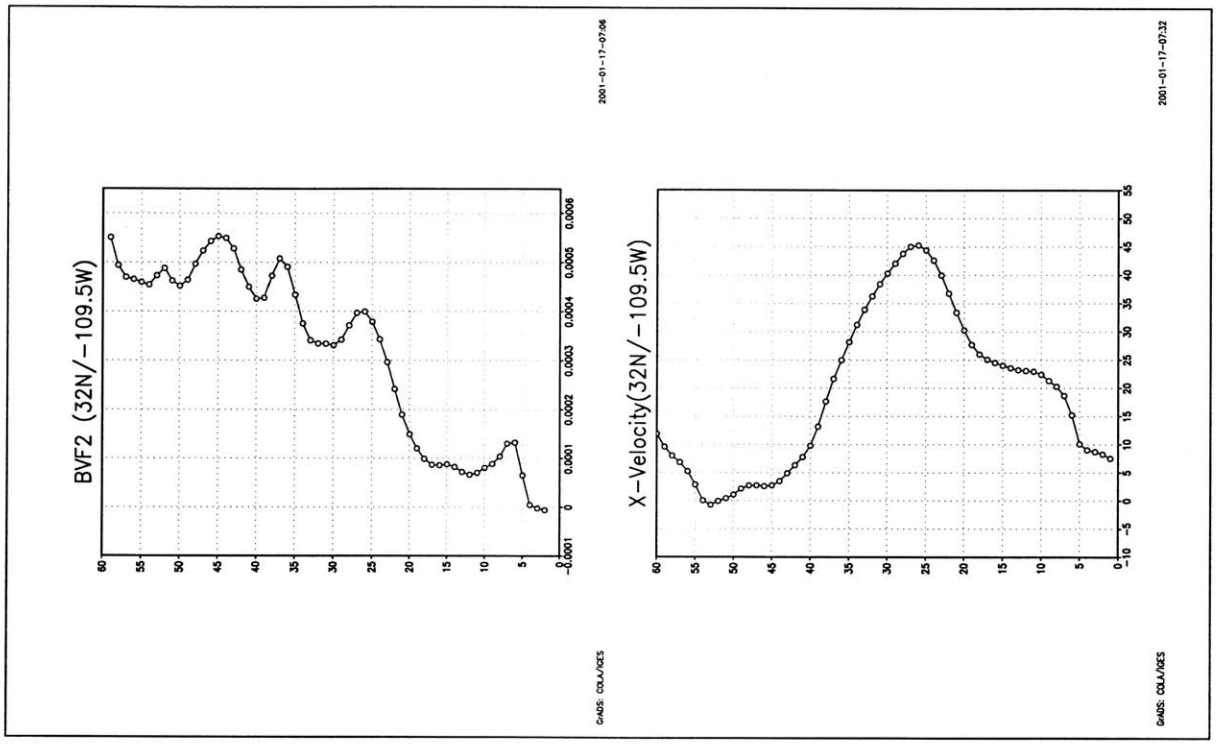

Figure A.3: BVF profile and x-velocity profile with tropopause at 15275km.

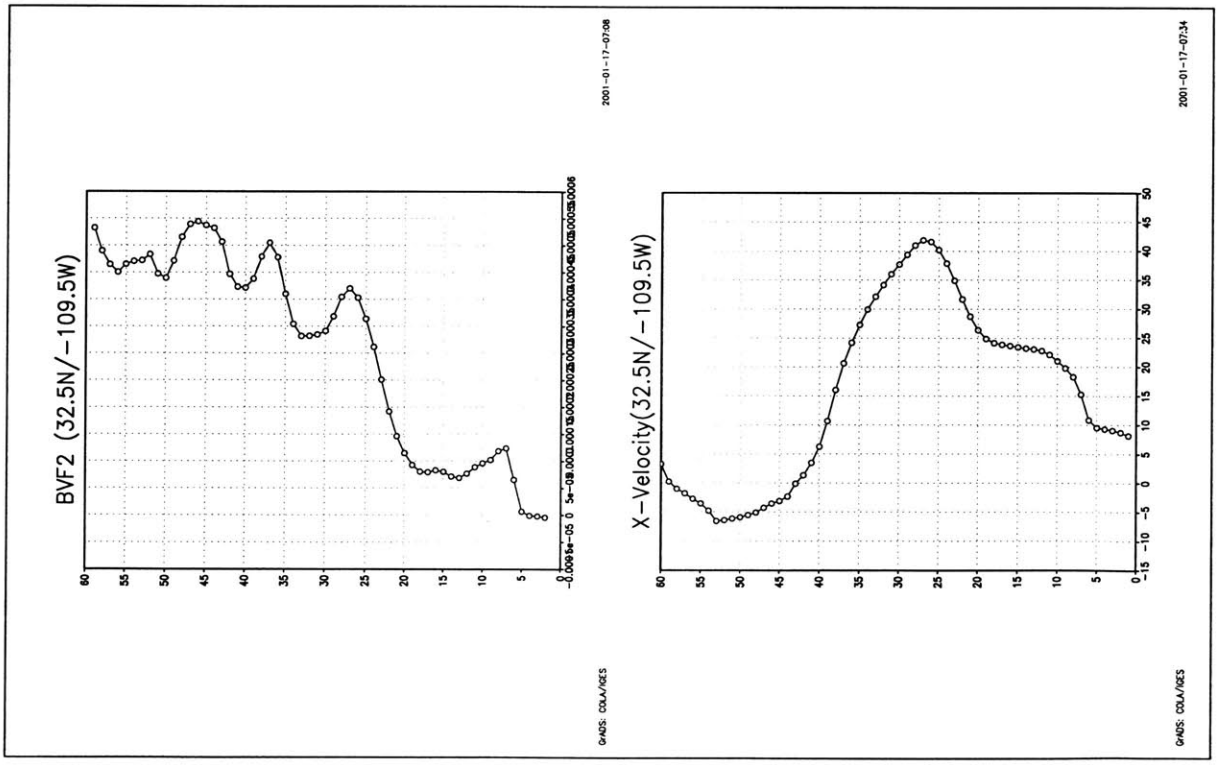

Figure A.4: BVF profile and x-velocity profiles with tropopause at 15579km.

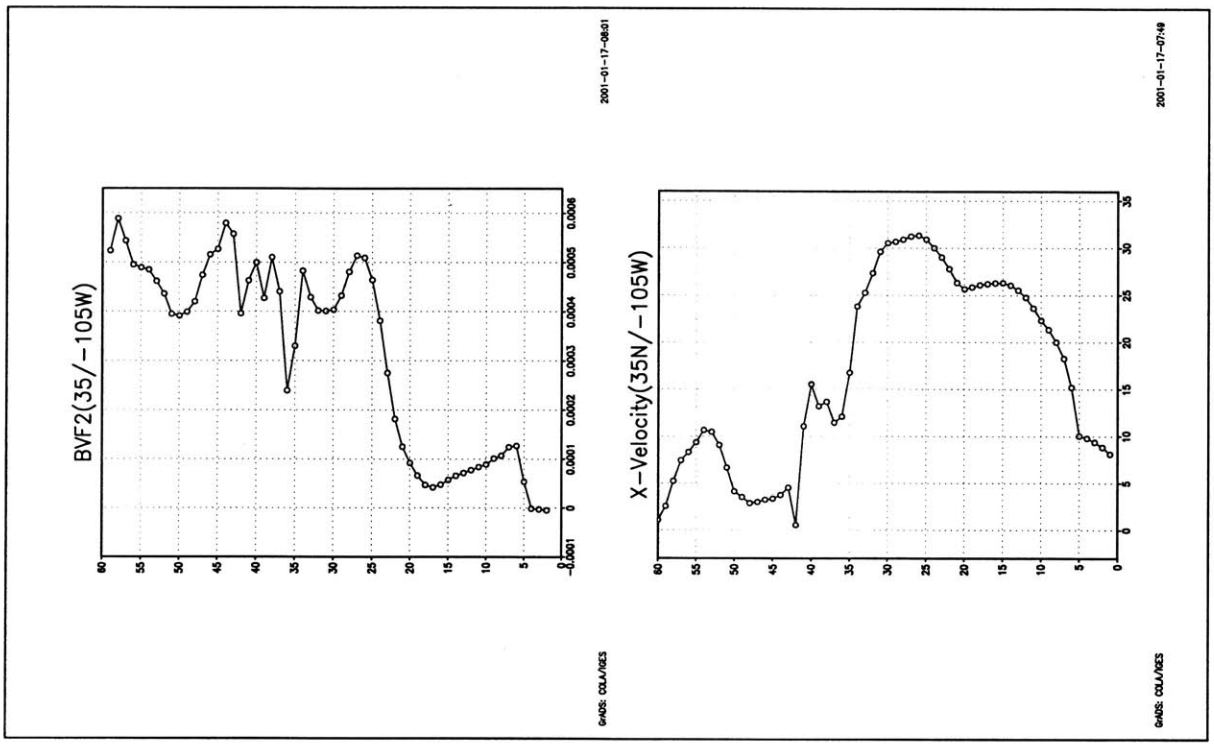

Figure A.5: BVF profile and x-velocity profiles with tropopause at 10635km.

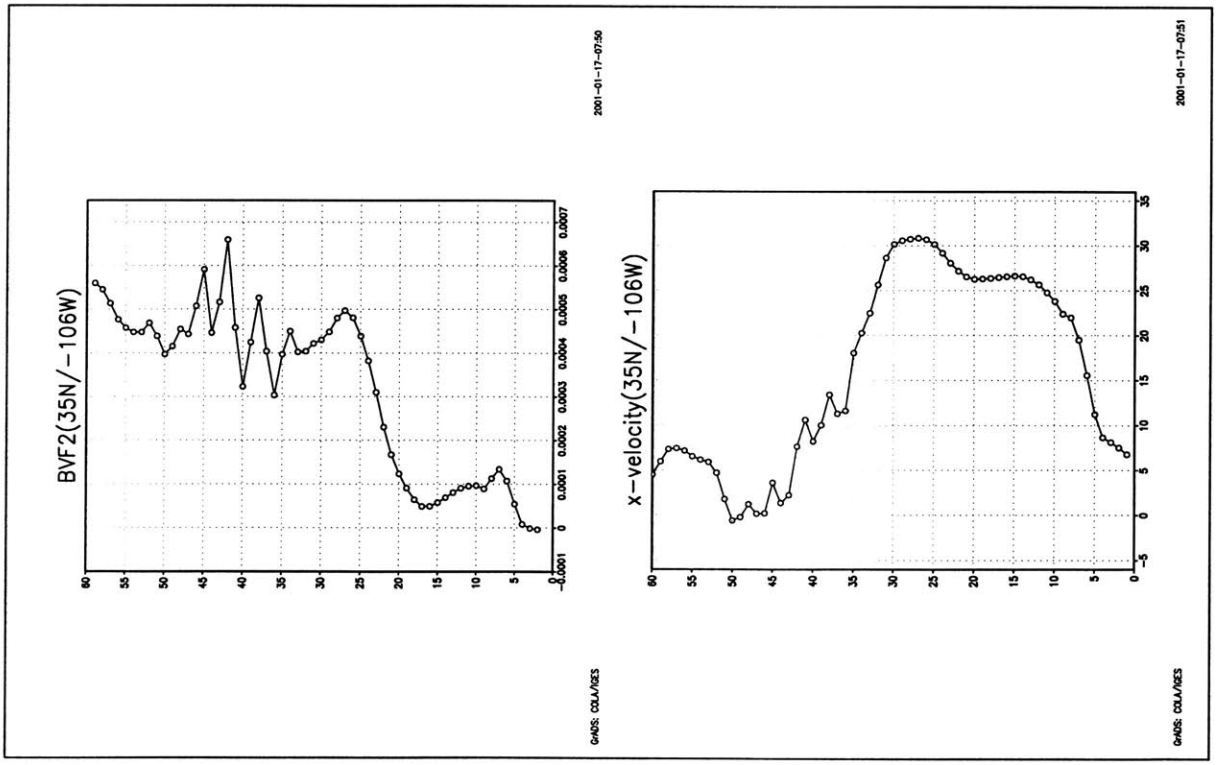

Figure A.6: BVF profile and x-velocity profiles with tropopause at 10442km.